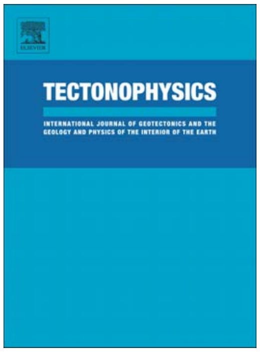

Buttressing and reverse reactivation of a normal fault in the Jurassic rocks of the Asturian Basin, NW Iberian Peninsula

H. Uzkeda, M. Bulnes, J. Poblet, J.C. García-Ramos, L. Piñuela

PII: S0040-1951(13)00256-4
DOI: doi: 10.1016/j.tecto.2013.04.012
Reference: TECTO 125865

To appear in: *Tectonophysics*

Received date: 8 February 2013
Revised date: 8 April 2013
Accepted date: 10 April 2013

Please cite this article as: Uzkeda, H., Bulnes, M., Poblet, J., García-Ramos, J.C., Piñuela, L., Buttressing and reverse reactivation of a normal fault in the Jurassic rocks of the Asturian Basin, NW Iberian Peninsula, *Tectonophysics* (2013), doi: 10.1016/j.tecto.2013.04.012

Buttressing and reverse reactivation of a normal fault in the Jurassic rocks of the Asturian Basin, NW Iberian Peninsula

Uzkeda, H.[1*]; Bulnes, M.[1]; Poblet, J.[1]; García-Ramos, J.C.[2] and Piñuela, L.[2]

[1] *Departamento de Geología, Universidad de Oviedo, C/Jesús Arias de Velasco s/n, 33005 Oviedo, Spain. E-mail (Uzkeda): hodei@geol.uniovi.es, e-mail (Bulnes): maite@geol.uniovi.es, e-mail (Poblet): jpoblet@geol.uniovi.es*

[2] *Museo del Jurásico de Asturias (MUJA), Rasa de San Telmo s/n, 33328 Colunga, Spain. E-mail (García-Ramos): jcgramos.muja@gmail.com, E-mail (Piñuela): lpinuela.muja@gmail.com*

** Corresponding author. Tel: +34 985 103120. Fax: +34 985 103103*

Abstract

A detailed structural analysis was carried out on the Jurassic rocks cropping out along the cliffs of La Conejera Inlet (Asturias, Spain). It includes a geological map and a distortion-free cross-section constructed via photogrammetric methods. La Conejera Inlet is located within the Asturian Basin, a Permian-Mesozoic extensional basin partially formed during the opening of the Bay of Biscay. It suffered selective basin inversion during a Cenozoic contraction responsible for the Pyrenees and its western prolongation along the north margin of the Iberian Peninsula. The study of the structures (folds, faults, joints and veins) of the hangingwall of two normal faults with opposite dip senses reveals that it underwent a later compressional stage in which one fault block acted as a buttress. The contractional deformation in the hangingwall, interpreted as a deformed rollover anticline with an associated antithetic fault, diminishes on moving away from one of the main faults. The positive inversion tectonics produced not only a buttressing effect, but it also involved a certain amount of reverse reactivation of one of the main faults that still preserves a normal displacement. The original normal motion would have taken place during the Middle?-Late Jurassic, related to an embryonic stage of the opening of the Bay of Biscay. The later contractional stage would have been caused by the Cenozoic Alpine shortening. The good outcrop quality allows a relative chronology for the observed structures to be established. Employing all the available information we tried to reconstruct the structure at depth and predict the detachment depth, and to estimate the amounts of extension (the present-day value and that before the compression) and compression.

Keywords: inversion tectonics, buttressing, fault reactivation, Jurassic.

1. INTRODUCTION

The Asturian Basin is an extensional basin filled by Permian-Mesozoic sediments that lay unconformably over a pre-Permian basement deformed during the Variscan Orogeny (Figure 1). This basin was partially inverted during the Cenozoic as a result of the contraction that formed the Pyrenees and its western prolongation along the northern margin of the Iberian Peninsula. Though some of the main structural features of the basin have been described in the literature, there is still a lack of understanding of the importance of the extensional and contractional structures that define the current anatomy of the basin, especially of its eastern sector (Gervilla et al., 1973; Pignatelli et al., 1973; Suárez Rodríguez, 1988; Lepvrier and Martínez-García, 1990; García-Ramos et al., 2006; Alonso et al., 2009; Uzkeda et al., 2010). Because of the abundant vegetation cover present in Asturias, the cliffs along the coast are the best places to study the geology of the region. For this work, we chose the cliffs of La Conejera Inlet (La Coneyera in Asturian language), situated on the central-eastern coast of Asturias. This site offers a nearly complete view of the hangingwalls and footwalls of two decametre-scale normal faults affecting Jurassic rocks with evidence of a buttressing effect during a later contractional stage.

The buttressing phenomenon has been studied mainly using large scale in subsurface examples, using seismic profiles or 3D volumes, and on regional-scale geological cross-sections (e.g., Flöttman and James, 1997; Cortés et al., 1999; Bailey et al., 2002; Potma and Betts, 2006). Detailed analysis of outcrop-scale faults and their related structures are few in number (for example, Dart et al., 1995; Knott et al., 1995 Glen et al., 2006; Rodríguez et al., 2008).

The field data obtained at La Conejera Inlet permitted the construction of a geological map and a distortion-free cross-section. The strategy outlined in this work enables the realization of a detailed structural analysis, including: characterizing the structures and establishing their relative chronology; proposing different models for the structural evolution of the region, during both the extensional and the contractional events; determining the lateral extension of the structures; defining a range of ages for their activity; make hypotheses about the detachment depth and the amounts of extension and compression; and integrating everything into a regional tectonic setting.

Understanding the geometry and evolution of the structures at La Conejera Inlet may provide new data for the understanding of regions with similar features. By using La Conejera as an analogue of inversion tectonics, it may also assist with the geological mapping of other less well exposed parts of the basin.

2.- GEOLOGICAL SETTING

The studied zone is part of the Asturian Basin, an emerged portion of the continental margin of North Iberia. This basin has an infilling of Permian-Mesozoic sediments uncomformably deposited on top of a Paleozoic basement. The age of the basement rocks ranges from Cambrian to Carboniferous. They belong to a fold and thrust belt located in the foreland of the Variscan Orogen of W Iberia, known as the Cantabrian Zone, generated mainly during the Carboniferous. This basement, as well as the Permian materials and the lower part of the Mesozoic cover, have undergone several tectonic episodes, mainly extensional, from Permian to Early Cretaceous (Lepvrier and Martínez-García, 1990; García-Ramos, 1997) related to a Permian-Triassic continental rifting (Malod and Mauffret, 1990; Quesada and Robles, 1995) and to the Upper Jurassic-Cretaceous opening of the Bay of Biscay (Robles et al., 1989, 1996; Quesada and Robles, 1995; Hernández, 2000; Aurell et al., 2002, 2003). These rocks together with later Mesozoic and Cenozoic ones were deformed by the Alpine contraction resulting from the convergence of the Iberian and Eurasian plates that, in this region, took place during the Cenozoic (Alonso et al. 1996). Apart from the Pyrenean Range, this contraction caused the uplift and partial inversion of the Asturian Basin through reactivation of some previous structures (Alonso et al., 1996; Pulgar et al., 1999). The evolution of this portion of NW Iberia continued with the episodic uplift of marine abrasion platforms (Flor, 1983; Mary, 1983; Álvarez-Marrón et al., 2008 amongst others) and neotectonic activity recorded by small magnitude seismic events (López-Fernández et al., 2004) and faults that involve Quaternary deposits (Gutiérrez-Claverol et al., 2006).

3.- METHODOLOGY

An exhaustive field campaign was carried out taking measurements (orientations, angles, dimensions) of structural elements such as folds and fractures, as well as beds. In addition, several sketches and geological interpretations of conventional photographs were carried out. This information formed the basis of a geological map and carry out a detailed structural analysis (Figure 2). Simultaneously a geological cross-section was constructed along the structure employing photogrammetric techniques (Martín et al., 2013) (Figure 3) aiming to:

a) locate accurately the stratigraphic and structural data collected in the field;

b) visualize the whole structure without any distortion and in an appropriate direction considering its characteristics;

c) measure distances and geometrical parameters related to folds and faults hard to take in the field because of for example difficulties of access, being at the highest parts of the cliff;

d) calculate values of displacement (extension and shortening) accommodated by the structures; and

e) reconstruct, via graphical and numerical techniques, the geometry of the structures at depth.

The cliff where the main faults and their related structures crop out has entrants and salients, and is oblique to the dominant direction of the structure making a three-dimensional approach essential. To achieve this we employed the photogrammetric software Stereo Rectification (see http://www.ideascad.es for further information), which uses the OpenCV library (Bradski and Kaehler, 2008), and Visage (Martín et al., 2007). The procedure consisted of taking photographs along the cliff with a calibrated camera that permitted the creation of stereoscopic pairs using the software Stereo Rectification. These pairs were later interpreted from a geological point of view using the software Visage. The resulting interpretations were scaled, orientated, and located in their actual coordinates through geo-referenced control points taken in the field with a total station and differential GPS. They were merged together and projected onto a plane following a direction perpendicular to the fold axes and parallel to the direction of tectonic transport. Two independent sections were created (section AA’ and BB’ in figure 2) using different directions of projection. The two sections were merged via a common fold limb.

4.- MAIN CHARACTERISTICS OF LA CONEJERA INLET

The cliff at La Conejera Inlet is approximately 225 m long and has a height that can reach 50 m. It has an orientation about NW-SE and is strongly inclined, near vertical in many points, to the NE (Figure 4).

The rocks that crop out along the cliff correspond to the lower (Buerres) and upper (Santa Mera) members of the Rodiles Formation (Valenzuela et al., 1986), with an age ranging from Early to Middle Jurassic (Suárez Vega, 1974). These two stratigraphic units, deposited in an inner carbonate ramp setting, have abundant fossil remains (brachiopods, bivalves, ammonites, belemnites, crinoids, gastropods and vertebrates), and are, basically, an alternation of grey marls and limestones. The main differences between both members are the nodulose character and higher limestone to marl ratio of the lower member (which makes it a more competent unit than the upper member), in contrast with the greater abundance of marls and planar-parallel beds of the upper member.

The earthquake databases of the National Geographic Institute (freely available at http://www.ign.es) and of the GASPI research project (López Fernández et al., 2004) document no recent activity in the zone.

In the cliffs of La Conejera Inlet a number of folds and faults (of normal, reverse and strike-slip types) with diverse orientations and dimensions have been recognized, as well as other structures such as joints and veins affecting the Jurassic rocks. The main structures of the region are two faults (Figures 2 and 3) with normal slips, limiting a sector of special interest where the deformation is concentrated. In outline, the beds in this area are folded by a double-hinge anticline of decametre-scale. The stratification in the footwall of the northern fault dips gently to the NW, whereas it is practically horizontal in the footwall of the southern one.

The northwesternmost main fault is a normal fault striking approximately NE-SW (the orientations measured in the field vary from N050E to N059E) and dipping from 55º to 75º to the SE. The stratigraphic separation caused by this fault, at the cliff foot, is estimated in about 58 m to 66 m, employing the Sinemurian-Pliensbachian boundary (Lower Jurassic) as a marker horizon (see the stratigraphic section constructed by Comas-Rengifo et al., 2010) (Figure 3c). The fault separates the Santa Mera Member (in the hangingwall) from the Buerres Member (in the footwall). In addition, the fault is the boundary between two zones with different amounts of strain, being much more significant in the hangingwall. The other main fault, located to the SE, has almost the same strike as the northwestern one and dips around 80º to the NW. Just as the other fault it separates the Santa Mera Member (in the hangingwall) from the Buerres Member (in the footwall) but the stratigraphic separation is slightly smaller, about 45 m. To estimate this value the Sinemurian-Pliensbachian boundary was again employed, but its stratigraphic position in the footwall of the southern fault had to be inferred from a key bed within the Asturian Lower Jurassic rocks assuming that the thickness between the Sinemurian-Pliensbachian boundary and the key level is constant along the outcrop at La Conejera Inlet. This key level has a large number of deformational sedimentary structures (loadcasts, convolute bedding, slumps and pseudo-nodules) and can be mapped across virtually the whole basin (García-Ramos et al., 1989) (Figure 3c).

The southern limb of the double-hinge, decametre-scale anticline dips about 30º-40º to the SE, whereas the northern one dips around 40º-50º to the NW. Both limbs are separated by a central region where stratification is sub-horizontal. This fold is affected by a number of sub-vertical faults inclined to the NW and the SE. The morphology of both the northern limb and the middle limb of the double-hinge anticline is modified by smaller, metre-scale, folds. The north limb of the double-hinge anticline terminates against the main northern fault. Towards the S, a monocline syncline adjacent to the double-hinge anticline appears. Near the main southern fault beds show a gentle dip to the SE and display a very smooth, decametre-scale anticline in between the main southern fault and the monocline syncline. A bend seems to control the strike of the hangingwall beds, as well as of the faults and the fold axes (Figure 2), since stratification passes from striking NE-SW in the NW to approximately ENE-WSW in the SE.

5.- MINOR STRUCTURES

5.1.- Hangingwall of the two main faults

The hangingwall is limited by the two main normal faults described above that dip in opposite senses and exhibit strikes approximately NE-SW. Most of the outcrop-scale deformation visible along the cliffs of La Conejera Inlet is concentrated here. However, its distribution along this fault block is not uniform. There is a gradual transition from the southern edge to the northern one, going from a region slightly deformed to another one pretty deformed by numerous folds and faults of diverse types (Figures 2 and 3). The deformation increases in the hangingwall towards the proximities of the northernmost main fault.

5.1.1.- Fractures

Four families of fractures (faults and joints) can be identified (Figures 5 and 6). The joints, which frequently have a calcite infilling, seem to be the oldest set and may be divided into two different sub-sets. The first one strikes approximately NW-SE (between N122E and N158E) and has elevated dips (greater than 70º) to the NE. The second sub-set has strikes ranging from N-S to NNE-SSW (from N177E to N200E, and most of them between N190E and N200E) and subvertical dips (85 to 90º) to the E and to the W (Figures 5a and 6).

A later set of fractures corresponds to normal faults striking NE-SW (from N036E to N093E, with the maximum between N050E and N060E) with a wide range of dips, from 45º-86º, with a mean of 65º, to the SSE and NNW (Figures 5b and 6). These faults can be mapped along the cliff for more than 15-20 m in some cases, although, commonly, their lengths do not exceed 5 m and their displacements are less than 1 m, typically of a few decimetres. It is probable that some faults have greater dimensions, as it has been attempted to illustrate on the map in figure 2. The normal faults tend to show planar geometries (sometimes distorted by displacements along bedding surfaces the product of, probably, a later flexural-slip) and, on these planes, kinematic indicators of two different movements may coexist. There are nearly pure dip-slip striae and younger striae with an important strike-slip component (recognized as left-lateral in many cases). These normal faults cut and offset the joints described above.

A third set of fractures consists of reverse faults striking ENE-WSW (from N024E to N093E, most of them between N060E and N070E) whose dips range from 6º to 57º both to the NNW as well as to the SSE (Figures 5c and 6). The striae associated with such faults indicate an almost pure dip-slip fault motion. The strike of these faults is practically coincident with that of the normal faults described above. In this group, two types of fractures may be differentiated: reverse faults with moderate to steep dips and large dimensions (over 25 m long at the outcrop) and gentle dipping thrusts of smaller sizes (except for some located close to the main southern fault that can be mapped for more than 20 m along the cliff). The first set could correspond to former normal faults reactivated as reverse. Thus, we have found faults with normal slips whose striae indicate a reverse left-lateral reactivation (pitch of 75º), though it is not possible to determine the amount of displacement caused by the fault reactivation. Thrusts are new generation structures developed to accommodate shortening. Generally, these thrusts show ramp-flat geometries and cause small displacements, though some examples may display displacements of even 3 m. Commonly, they cut and offset older normal faults (Figure 7); nevertheless in some cases the reverse faults may appear displaced by the reactivated normal faults. This fact could be explained assuming that the reverse faults post-date the first movement of the reactivated faults (normal) but pre-date the second one (left-lateral strike-slip). On the surfaces of these reverse faults and thrusts we have not found evidence of reactivation as strike-slip faults, however, this does not imply that they could not have acted in such way. The reverse faults and thrusts are the most important fractures in terms of extension and abundance in the zone close to the main faults.

The last set of fractures are faults whose dominant striae indicate right-lateral motion and seem to cut and offset the other sets. They strike approximately NW-SE (from N095E to N148E, most of them between N100E and N120E) and their dips range from 40º-88º to the NE or SW (Figures 5d and 6). The dimensions and displacements of these faults are difficult to assess because their surfaces tend to be coincident with the cliff faces, so one of their fault blocks is usually missing. The orientation of these strike-slip faults coincides, broadly, with that of some large-scale normal faults identified in nearby regions (Figure 1b). Therefore, it cannot be discarded that these right-lateral faults come from inherited normal faults reactivated. Indeed, on one of these fault surfaces we found evidence of having acted as a normal fault prior to the right-lateral movement (Figure 5d).

The strikes of the fractures show a certain bend from the proximities of the main northern fault to the SE (Figures 2 and 8). This is especially evident for the normal faults that pass from strikes predominantly NE-SW (Figure 8a) to orientations more ENE-WSW (Figure 8b); and the right-lateral faults that change their WNW-ESE disposition (Figure 8a) to an almost NW-SE one

(Figure 8b). The geological map (Figure 2) shows how the bedding exhibits this rotation too, and, in turn, the axes of the folds affecting it (Figures 2 and 8).

The number of fractures increases towards the main northern normal fault, concurrently with the quantity of deformation (Figure 3). To quantify this observation we estimated the fracture intensity (taken as the accumulated fault length divided by the studied surface) in three regions (Figure 3): close to the main northern fault, next to the main southern one and between both. We chose an area sampling over the total of the interpreted surface. The results are: 0.79 m/m^2 for the northernmost area; 0.22 m /m^2 for the central one; and 0.13 m/m^2 in the southernmost part. In the footwalls of the main faults the fracture intensity is about 0.12 m/m^2.

Figure 9 shows graphs for eight minor faults situated at the hangingwall of the main faults (Figures 2 and 3). Five reverse faults (F2, F3, F4, F7 and F8) and three normal faults (F1, F5 and F6) without evidence of strike-slip reactivation were selected (Figures 2 and 10). The measurements of both the displacements and the distances were performed directly on the distortion-free cross-section of Figure 3. An arbitrary point on each fault trace (usually the upper fault tip or the limit of the outcrop) was selected as reference point. To deal with the inherent difficulties of working with structures of different sizes we normalized the resulting graphs using the maximum distance along the fault as the denominator, thus, the distances along the fault will range from 0 to 1, whereas the displacements will vary between 0 and 0.6 (in most cases about 0.15). Three basic patterns can be identified in the diagrams:

a) The displacement is approximately constant along the fault plane, such as fault F4 graph (Figure 9d).

b) The displacement increases from the reference point (faults F1(Figure 9a), F2 (Figure 9b), F6 (Figure 9f) and F8 (Figure 9h)). Nevertheless, there are segments where the displacement remains constant (as, for instance, F1, F2 or F6).

c) Faults whose functions depict an inverted “V”. The displacement grows until reaching a maximum value and then it decreases, (faults F3 (Figure 9c), F5 (Figure 9e) and F7 (Figure 9g)). The intersection of the function extremes with the x-axis could provide a tentative estimate of the position of the fault tips.

Some faults are developed within a stratigraphic sequence consisting of an alternation of materials with different competencies (marls and limestones) and it seems that the greater displacement changes take place, in general, in marly levels, being more constant in the limestones. Nevertheless, these changes are independent of the cut-off angles between bedding and the faults.

5.1.2.- Folds

In addition to fracture data, we collected specific information for a total of 19 folds (the biggest ones of the outcrop) of decimetre to metre-scale (Figure 10). In the field we took data for 15 folds (6 synclines and 9 anticlines), whereas the remaining 4 folds were studied using photogrammetry. The axial surface traces of the larger folds were drawn on the geological map (Figure 2). These traces tend to be sub-parallel or slightly oblique to the faults nearby.

Using the measurements taken we calculated parameters such the orientations of the fold axes, interlimb angles, amplitudes and half-wavelengths (Figure 11 and Table 1). Data shown in table 1 indicate that they are metre-scale folds, with half-wavelengths from slightly less than 1 m to more than 5 m, and maximum amplitudes slightly greater than 1.5 m, with the exception of two folds (XVII and XVIII) that are larger (wavelengths of 16 m and amplitudes of about 3 m) (Table 1). These folds display commonly rounded hinges, though some may show a somewhat more kink-like geometry (e.g. fold IX) and they are parallel folds without bed thickness changes. However, some thrusts in the hinge zones (Figures 6, 7 and 12) may thicken these regions. We estimated the degree of cylindricity of the folds by observing the dispersion of the stratification poles taken in the field from the cylindrical best-fit plane (Ramsay, 1967). In all cases most of the data are close to the best fit plane, and therefore, the structures can be considered as cylindrical (Figure 13). The fold axes have orientations from NE-SW to E-W and plunge less than 10º to the W or SW (except for fold X that is inclined to the NE, and folds III and II with plunges to the SW of 20º and 27º respectively) (Figures 8 and 10 and Table 1), so they would be horizontal according to the classification of Fleuty (1964). According to Fleuty (1964) classification for interlimb angles the folds would be open because the angles vary from 73º (fold VII) to 130º (folds XVIII and XIX) (Figure 11 and Table 1). All the folds have limbs dipping in opposing senses. Considering the classification of Fleuty (1964), and taking into account the orientation of the axial planes (Table 1), the folds analysed would be upright (folds III, VII, X, XII, XIII, XIV, XV, XVI, XVII and XVIII), with strongly inclined axial plane (folds I, II, V, VI, VIII, IX and XI) and with moderately inclined axial plane (folds IV and XIX).

The analysis of the fold axes permitted the recognition of a bend from the NW to the SE of the studied area, similar to that shown by the stratification and some of the fractures. Thus, the fold axes, NE-SW oriented in the northern sector (Figure 8a), become almost E-W in the southern portion (Figure 8b). This was the main reason for constructing two cross sections (AA' and BB' in Figures 2 and 3) employing two different vectors of projection of data onto the cross-section planes chosen. The mean axis for the northernmost folds (folds I to XVII) has an orientation 244/09, whereas the mean axis for the folds XVIII and XIX is 268/02.

The fold distribution is not uniform along the hangingwall of the main faults, being more frequent closer to the northern main fault, where the deformation is more intense (Figure 10).

A parameter that varies progressively on moving away from the main northern fault is the interlimb angle (Figure 11). In the closer sectors (up to 15 m from the fault) this angle ranges from 69º to 95º, with a mean around 80º (fold I to VIII); a bit farther (from 30 m to 90 m away from the fault, folds IX to XVII) the mean interlimb angle increases to 112º (the values range from 107º to 127º); whereas in the most distant sector (folds XI and XII) the interlimb angle is about 130º (Figure 11). Broadly, it can be concluded that the folds become gradually more open towards the sectors where the folds and faults are less frequent, i.e., where the strain is less intense.

Another parameter that can reflect the variation in the strain intensity is the relation between the amplitude and the half-wavelength of the folds (Figure 11). The measurements necessary to make these calculations were taken directly from the cross section of figure 3. In the case of folds cut by faults, the fold limbs have been prolonged to measure the half-wavelength. This ratio offers information comparable to that provided by the interlimb angle, given that it indicates the tightening degree of the folds. Tight folds have high amplitude to half-wavelength ratios, whereas open folds have smaller ratios. Close to the main northern fault (distance of less than 15 m from the fault, folds I to VIII) the ratio ranges from 0.39 to 0.76, with a mean value of 0.53. In more remote sectors this parameter ranges from 0.07 to 0.34 with a mean value of 0.20, being always less than 0.20 at distances farther than 50 m away from the fault. The obtained results are consistent with the interlimb angles (Figure 11).

5.1.3.- Fold-fault relationships

Some folds are bounded by faults with moderate to steep dips (both normal and reverse); as folds IX, XI and XII (Figure 10). In these cases, the genetic relationship between folds and faults is not very clear. It is probable that the faults acted as hard-to-deform surfaces and that the area bounded by them deformed by folding.

In some cases a huge concentration of faults (normal, reverse and strike-slip) may be found within the fold hinge zones, as in the case of folds XVI (Figure 12) and XVII (Figure 7). The surface of a large number of normal faults, as well as of joints and veins, were cut and offset along bedding surfaces that seem to have acted as slip planes. For example, some normal faults developed across syncline XVI exhibit staircase geometry, with little displacements along bedding planes (Figure 12). Actually, there is evidence, such as striae on the bedding planes, that prove that there was motion along them. The displacements measured using cut-off points of faults as indicators, as well as the displacement senses indicated by the striae are consistent with a flexural-slip model. This suggests that flexural-slip is an important mechanism of distribution of strain along folded layers in the study area. This leads us to reject an alternative explanation for the staircase geometry of the faults based on their refraction when crossing levels of different rheological behaviours documented in other regions (e.g., Schöpfer et al., 2007). The observation above would indicate that the normal faults, joints and veins are older than folding and, consequently, there would be no genetic relationship between them. Anticline XVII (Figures 7 and 10) is one of the best examples for determining the temporal sequence of the folds and faults. The normal faults and thrusts vary their inclination depending on the structural position they occupy along the fold (Figure 7). The north-directed thrusts dip to the S in the southeastern fold limb, and decrease their dips on moving to the northwestern fold limb, reaching even dips with opposite sense. The normal faults show an analogous situation; there is a set of faults originally parallel (they all form virtually the same angle with the stratification) that increase their dips as passing from the southeastern fold limb to the northwestern one.

There are also fault-related folds, e.g., the fold XIX developed on the ramp of one of the south-directed thrusts close to the southeastern limit of the hangingwall (Figure 10). The displacement decreases towards the upper fault tip, together with the fold geometry, suggests that it could be interpreted as a fault-propagation fold (Figure 14). In addition, some folds only partially outcropping (folds XII, XV and XVII) may be related to faults located at deeper levels.

In syncline XVI (Figure 12) there is a slightly folded thrust affecting both fold limbs.

All these observations would indicate that the thrusts are genetically related to the folds and are, in a broad sense, simultaneous structures. They might have initiated barely before the folding, during it or at its late stages.

Although there does not seem to be a genetic relationship between the folds and strike-slip faults, their temporal relationship is unclear as insufficient evidence has been found in the field.

5.2.- Footwalls of the main faults

The strain in the footwall of both main normal faults is much less intense than in their common hangingwall (Figures 2 and 3). The bedding dips gently, between 5º and 25º to the NW, and is affected only by one set of joints and two sets of faults of minor significance (Figure 15). The joints are easily recognized in the cliff faces because they generate surfaces covered by calcite, with crystals growing approximately perpendicular to the fracture planes. These joints have NW-SE strikes (ranging from N135E to N155E) and steep dips (well above 75º) to the NE and the SW (Figure 16a).

Another set of fractures includes normal faults striking NE-SW (between N048E and N088E, most of them between N070E and N080E) and dipping from 42º to 88º indistinctly to the NW and to the SE (Figure 16b). The presence of two sets of striae on the fault surfaces is common (though it is not always possible to take measurements): an older one that indicates a normal dip-slip movement and a later one of a left-lateral slip. These faults can be mapped, in some cases, for more than 10 m on the cliff and show displacements typically lesser than 1 m. Geometrically they are rather planar, without significant dip changes; in occasions these faults conform conjugate systems (Figure 17).

The third group of fractures consists of right-lateral strike-slip faults striking E-W (from N095E to N105E) and dipping more than 75º to the N as well as to the S (Figure 16c). They are shorter than the normal faults, submetre to metre-scale, being hard to estimate their displacements. Contrary to the other fracture sets, this family does not show a calcite infilling.

From cross-cutting relationships, especially clear on bedding planes (Figure 18), a relative chronology can be deduced. The oldest structures are the joints, then the normal faults (some of them reactivated as left-lateral) and, finally, the right-lateral faults. The relative timing of the right-lateral faults and the left-lateral movement of the normal faults remains unclear.

6.- INTERPRETATION OF THE GENERAL GEOMETRY

The overall geometry of the beds in the hangingwall of the main faults, with sub-horizontal strata at the southern extreme that pass to a double-hinge anticline with beds moderately inclined towards the northern fault near the fault (Figure 3), could correspond to a rollover anticline associated with this fault during extension, which would have been deformed later. If this interpretation were correct, the northern fault would probably reach a detachment level at depth, with the other fault (with less displacement) being antithetic. This second fault may define the boundary between the region only transported along the detachment level and the sector folded and extended forming the rollover. In this situation a half-graben would be defined (Figure 19a). If the rollover geometry had not been distorted by later structures, it would be relatively easy to determine the full geometry of the northern main fault applying published techniques to reconstruct the geometry of normal faults at depth. There is an alternative explanation for this region in which both main faults would define an asymmetric graben (Figure 19b), so that the extension would have been accommodated in their common hangingwall via minor structures, including a certain amount of folding and/or pure shear. The smaller displacement of the southern main fault and the second-order faults in the hangingwall creating stair steps would cause the bedding to acquire a dip to the NW. In this alternative interpretation both main faults would join a detachment level under the topographic surface. This second model fails to reproduce the progressive dip variation the beds show along the hangingwall with the absence of steps limited by faults. As a consequence, we think that it is less suitable than the model above, and therefore, it will not be taken into account for future considerations.

Despite that the main faults are normal, their common hangingwall contains reverse faults and folds characteristic of compressive zones plus strike-slip faults. This phenomenon contrasts with the situation in the footwalls where only normal and strike-slip faults occur without thrusts and/or folds typical of contractional regimes. This restriction of the shortening deformation in the main faults' hangingwall would suggest that at least one of the main faults must have acted as a buttress during a contractional stage later to its formation. The contrast of competence between both fault blocks, with more competent rocks in the footwall than in the hangingwall (where marls are more abundant) supports this interpretation. The distribution of the strain within the hangingwall also fits this kind of process, being greater in magnitude, with more abundant reverse faults and folds (Figures 3 and 10), tighter folds (Figure 11) and larger fracture intensity (Figure 3) towards the main northern fault (Figure 20). Towards the S, the contractional deformation terminates with folds and S-directed thrusts dipping in opposite sense to the main northern fault (Figures 3 and 14). This situation, documented in physical experiments of inverted listric faults and planar faults emanating from a detachment (e.g., McClay, 1989, 1995), reinforces our interpretation of La Conejera Inlet structures as a half-graben subsequently affected by positive inversion tectonics. As a result of the buttressing effect caused by the main fault, the rocks underwent an intense strain consisting of the development of new folds and thrusts of diverse scales. However, some of the older normal faults associated with the main faults were reactivated (faults planes with more than one set of striae) (Figure 5), others suffered a rotation caused by folding (Figure 7) and some of them were cut and offset by new faults and by bedding surfaces that underwent motion as a result of flexural-slip (Figures 12 and 20). This compression would be the responsible for the modified morphology of the main faults' hangingwall (Figure 3), which prevents the recognition of the asymmetric graben and of the rollover geometry related to the main northern fault that could have existed (Figure 19).

There are two basic structural models for the compressive stage (Figure 21) depending on the main faults behaviour. In the first one the folds and reverse faults would be fundamentally the result of buckling, though not completely pure since beds had a certain dip to the NW caused by the previous extensional tectonic event. According to this interpretation the main faults would not have been reactivated but they would preserve their original normal displacement, since the northern main fault would have only acted as a buttress. However, a certain amount of reactivation of the detachment level is unavoidable. The folds would be basically structures developed over the detachment (Figure 21a). In the second interpretation (Figure 21b) buckling and reactivation of the detachment would have also taken place, but there would also be at least one anticline ("AC" in Figure 3b) as result from the reactivation of the main northern fault. This anticline would be a fault-bend fold caused by the transport of the beds over the footwall ramp of the northern main fault. If this interpretation were correct, the axial surface of the monocline syncline adjacent to this anticline, to the SE, would intersect the main northern fault where it passes from footwall ramp to flat, i.e. at the detachment level. This axial surface would be an active axial surface whose corresponding inactive axial surface would be represented by the anticline axial surface situated more to the NW (Figure 21b), according to the fault-bend fold model of Suppe (1983). Accepting this interpretation, the distance between these axial traces (about 12 m) would reflect the amount of reverse reactivation of the main northern fault. The southern main fault would not have been reactivated in this model.

In the description of the minor structures developed in the hangingwall of the main faults we made reference to the existence of normal faults reactivated as strike-slip faults (both right and left-lateral). Thus, second order faults striking NW-SE were reactivated as right-lateral, whereas the NE-SW faults acted as left-lateral. Their orientations and movement senses would be consistent with a compression approximately N-S (Figure 22). Such compression would be also consistent with the reverse faults and thrusts identified (Figure 22). Considering this, it is probable that the main faults at La Conejera Inlet would have suffered a certain amount of reactivation as left-lateral faults. Additionally the bend that the structures (folds and faults) and the stratification show from NW to SE in the hangingwall of the main faults could be related to such N-S compression.

7.- CARTOGRAPHIC EXTENSION OF THE MAIN FAULTS

The outcrop quality diminishes substantially on moving away from the coastal cliffs because of the vegetal cover, making it very difficult to extend the geological features identified along the coast to the south. In the light of this problem, structure contours have been drawn to project the desired elements (stratigraphic contacts, faults) inland. Using such a procedure, it seems that the main faults cropping out at La Conejera Inlet follow, approximately, the Villaviciosa estuary (Figure 1b), where the Villaviciosa Fault is situated (Beroiz et al., 1972; Suárez Rodríguez, 1988). Though there is no cartographic continuity between the Villaviciosa Fault and the faults at La Conejera Inlet, there are some indications suggesting that they may be connected. On the sketch map of the main faults of the Asturian Basin by Lepvrier and Martínez-García (1990), the Villaviciosa Fault is interpreted as a Permian normal fault with small later movements. In the maps and cross sections produced by Beroiz et al. (1972) and Suárez Rodríguez (1988) the Villaviciosa Fault is a NE-SW striking structure with vertical or steep dip to the SE. It has a minimum cartographic length of 9 km running southwestwards from the W of the locality of Villaviciosa. Its possible continuation to the NE is hidden under the Recent sediments deposited within the Villaviciosa estuary. This fault separates, along a large portion of its trace, the lowermost Triassic rocks in the northwestern fault block from younger Triassic ones in the southeastern fault block. The bedding in both fault blocks dips gently (10-20º) to the N or NW. It is a fault that downthrows its southeastern fault block about 100 m according to Beroiz et al. (1972) (B-B’ cross section in figure 23) or about 70 to 105 m according to Suárez Rodríguez (1988) (A-A’ and C-C’ cross sections, respectively, in figure 23). The throw variation observed in different cross sections suggests a certain loss of displacement to the NE.

We also tried to extend the fault seawards, to the NE. Based on bathymetric information provided by the Hydrographic Institute of the Spanish Navy we created a raster of depth and a map with depth contours each 10 m (Figure 24a) and a slope map (Figure 24b). The slope map displays a NE-SW elongated zone of low inclination (green colours in the map) bounded by areas of greater slopes (yellow and red colours) near the coast. This fringe can be followed up to 6 km offshore, until reaching a zone, WNW-ESE oriented, of high inclinations (red colours in the map) located at a depth of about 100 m. From here to the NE some of the contours (light green colours) are interrupted (Figure 24b), which might indicate the fault prolongation even farther. In a distant location, the Lastres Canyon can be found (Figure 24c). Though it has the same orientation (at least its initial portion) as the Conejera Inlet fault, the large distance between it and the coast (around 50 kilometres) makes it risky to project the cartographic trace of the fault as far as this canyon.

8.- TECTONICS-SEDIMENTATION RELATIONSHIPS AND FAULT AGE

There is a noticeable difference between the stratigraphic column made by Suárez Vega (1974) along the Rodiles cliffs (in the footwall of the main northern fault) and the one constructed more to the E, next to Santa Mera (in the hangingwall of the aforementioned fault) (Figure 25). Whereas the top of the Rodiles Formation is of Lower Bajocian age in Santa Mera, it is noticeably older (Upper Toarcian) in Rodiles. The Santa Mera section is 30 m thicker than the Rodiles section (Figure 25). This variation suggests tectonic control over the sedimentation during the Middle?-Late Jurassic, although later tectonic activity could have taken place as well. A normal movement of the northern main fault at La Conejera Inlet is consistent with this scheme, providing that the thicker series is located in the downthrown fault block. With the available data three basic models can be proposed to explain the age of the normal fault activity (Figure 26):

a) In the first option the Rodiles Formation sedimentation would be equal in both fault blocks. The fault activity posterior to the Lower Bajocian but previous to the deposit of the overlying unit (Vega Formation of Kimmeridgian age), combined with partial erosion of the upthrow fault block would result in the present-day configuration (Figure 26a). The Rodiles Formation would be pre-tectonic respect to the normal movement of the fault.

b) Another explanation would be a fault movement coeval with the deposit of the upper part of the Rodiles Formation (from Upper Toarcian to Lower Bajocian) (Figure 26b).

c) The last option considers a fault movement restricted to Upper Toarcian. After this fault displacement the upper part of the Rodiles Formation would be deposited only in the accommodation space created in the downthrow fault block. The Upper Toarcian-Lower

Bajocian sediments would onlap over the fault plane (Figure 26c) and would be post-tectonic with regard to the normal fault movement.

We can conclude that part of the normal activity of the fault occurred, in any case, before the deposition of the Vega Formation assigned tentatively to the Kimmeridgian by Suárez Vega (1974), Schudack (1987), Schudack and Schudack (2002) and Pujalte et al. (2004) amongst others. This activity might have started during the Aalenian, an age when rapid lateral facies and thickness changes began to appear along the Asturian Basin (Fernández-López and Suárez Vega, 1981; Valenzuela et al., 1989), though most of the displacement could have taken place during the Late Jurassic, when the opening of the Bay of Biscay commenced (Robles et al., 1989, 1996, 2004; Quesada and Robles, 1995; Hernández, 2000; Aurell et al., 2002, 2003). Since the fault displacement before the sedimentation of the Vega Formation can be estimated in about 30 m, the fault necessarily moved again as normal (increasing its displacement between 28 and 36 metres) subsequently to acquire a displacement at least equal to the present-day one.

9.- DETACHMENT DEPTH CALCULATIONS

In a previous section, a structural interpretation is proposed to account for the extensional stage of the structure, which relies on a detachment level at depth. To calculate the depth of that level we have used methods based on area preservation and estimates of the amount of extension. A compendium of these techniques can be found in Poblet and Bulnes (2005). The main assumptions and difficulties posed by the application of these techniques to the study area are:

a) Plane strain is assumed. The tectonic transport vectors indicated by the striae of both normal and reverse faults (Figure 27) seemed sub-parallel and contained in the selected plane. However, there are striae showing a strike-slip displacement, which would imply some transport out of the cross section plane.

b) In the region studied, a compressional event is superposed on a previous extensional one. Despite the transport directions for both events are approximately coincident, the fact that they may have taken place through different deformation mechanisms may generate problems when applying the published methods because they are based on one independent mechanism. It seems that flexural-slip was an important mechanism during shortening, remaining uncertain which one would have acted during extension. If, for instance, vertical or inclined shear is chosen, it could happen that the most successful shear angle selected was not the one acting during extension.

c) We discarded for our calculations the amount of extension caused by second order faults, which seem of minor importance (Figure 10). As a consequence the calculated detachment will lie slightly deeper than if we had considered the smaller faults.

d) Most of the methods use pre-tectonic beds to estimate the detachment depth. The layers depicted in the cross section (Figure 3) used to make the calculations are assumed to maintain constant thickness. However, if some of them were growth strata with respect to the extensional activity of the northern main fault, as suggested in a section above, they would probably display thickness variations, and therefore, the detachment depth estimations would not supply accurate results.

The results of the application of the different techniques using five horizons are shown in figure 28. There is an alternative method to find out the detachment depth if the hypothesis of a certain reverse reactivation of the main northern fault is accepted. The geometry of the fault-bend fold resulting from the transport of beds along the footwall ramp would provide the information necessary. The intersection of the southernmost axial trace of this fold (TAS in Figure 28) with the prolongation at depth of the main northern fault would predict the position of the detachment level according to the fault-bend folding model (Suppe, 1983). If the structural interpretation for the extensional stage proposed is correct, according to physical experiments of listric and planar normal faults (see, for instance, McClay, 1989, 1995) the detachment level should not be deeper than the intersection between the main normal fault and the antithetic one. Therefore, this intersection would determine the maximum reasonable depth for the detachment level. Furthermore, the experiments show that the main antithetic faults emanate from the intersection between the main extensional fault and the detachment. These observations provide another way to estimate the detachment depth by area balance; the beds' area bounded by the detachment and both main faults in the deformed, present-day cross-section must be equal to that comprised between the main fault and the antithetic one in the undeformed cross-section. The detachment depth can be estimated by the trial and error method.

Once the different techniques have been applied it is time to decide which one provides the most reasonable solution.

The results obtained based on the displacement along the fault (Williams and Vann, 1987), and the linear best fit of previously calculated depths (Poblet and Bulnes, 2005) (Figure 30) can be rejected because they predict that the detachment should be observable in the field (Figures 28, 29 and 30).

The estimates obtained by the bed-length and heave methods (Gibbs, 1983) could be, in principle, acceptable as they fall under the topographic surface and within stratigraphic units with levels prone to act as detachments (Figure 28). The Bárzana Member, of Hettangian age, (Barrón et al., 2006) is an alternation of lutites, calcareous rocks (mainly dolostones) and evaporites, whereas the Keuper facies contain abundant anhydrite. However, the results achieved through different horizons have a wide spreading, making difficult to choose one of them as the most suitable one.

The depth to detachment that can be estimated with the lineal best fit of the lost area data (Groshong, 1994) meets also the requirements of being under the topographic surface and within a stratigraphic unit of appropriate lithology (Figure 28). Nevertheless, this method seems to show problems in this particular case as slight lost-area variations lead to important changes in the calculated depth, probably because the data do not represent a wide enough range to get a reliable fit.

The results provided by the inclined shear method (White, 1987), possess a number of characteristics pointing to their correctness. As recommended by White et al. (1986) and Xiao and Suppe (1992), the chosen shear dip (80º in this particular case) is the average dip of minor faults located at the hangingwall of the main faults. The depths calculated using different horizons are under the topographic surface, lie within an appropriate stratigraphic unit (Bárzana Member) and are relatively grouped (Figure 28), indicative of a good fit (Wihte and Yielding, 1991). An additional factor that supports this is that the detachments estimated using this method are in accordance with those obtained using the fault-bend fold model and the area balance based on knowing the original position of the faults. Taking this into account, this depth will be the one considered from now on to make any further calculations and observations. Nevertheless, the existence of a relatively shallow (less than 100 m under the topographic surface) detachment level at La Conejera Inlet requires an explanation for the alleged link between the main northern fault at La Conejera Inlet and the Villaviciosa Fault, since the sections made by Beroiz et al. (1972) and Suárez Rodríguez (1988) across the Villaviciosa Fault indicate that this fault affects deeper rocks. It may be that the detachment reaches deeper levels to the SW where, in addition, the fault displacement increases. Thus, the Villaviciosa-La Conejera Fault would have lateral and/or oblique ramps connecting adjacent flats. Another way to explain such variation would be oblique and/or transversal faults, similar to tear faults, which would accommodate the differences along the fault.

Faults of such a type have been mapped by Beroiz et al. (1972) and Suárez Rodríguez (1988) (Figure 1b and 23).

10.- EXTENSION / CONTRACTION ESTIMATION

Given that this region has undergone an old extensional event followed by a latter contractional one it is necessary to estimate both the extension and the contraction amounts. The remaining extension after the contractional event can be estimated measuring the separation between the two main faults along the detachment in the deformed, present-day cross-section (Figure 31a) as long as our hypothesis that they originally emanated from the same point at depth is correct. This distance is about 50 m (Table 2). To compute the contraction we removed the reverse displacement deduced from the separation of the axial traces of the fault-bend fold (aound 12 m, figure 31b and table 2) and then we calculated the shortening using bed lengths (approximately 20m, figure 31c and table 2), assuming that beds kept constant their lengths during contraction, and using area balance (about 28m, figure 31d and table 2), assuming plane strain. Adding these values to the present-day extension an estimation of the original amount of extension can be obtained (about 70-80 m, table 2).

11.- REGIONAL TECTONICS

The main processes that have taken place here since the Jurassic are related to three principal events: 1) Bay of Biscay opening from Late Jurassic to Early Cretaceous (maximum development during the Aptian); 2) simultaneous rotation of the Iberian Plate during Cretaceous times; and 3) posterior compression leading to the formation of the Pyrenees and its western prolongation along the N Iberian Peninsula during the Late Cretaceous and Cenozoic (see, for example, Ziegler, 1988; Sibuet et al., 2004; Handy et al., 2010; Vissers and Meijer, 2012). Considering the Middle?-Late Jurassic age determined for the faults at La Conejera Inlet, they could have formed during an embryonic stage of the extensional event linked to the opening of the bay (Figure 32a). Since the Iberian Plate experienced a 35º counter-clockwise rotation (Van der Voo, 1969; García-Mondéjar, 1996; Gong et al., 2008), it is reasonable to think that the faults would have originated with a more E-W orientation than the one shown nowadays (Figure 32b). During the Alpine contraction of broadly N-S direction (Figure 32c), reactivation of the faults (as reverse or strike-slip faults depending on their position respect to the principal stress axes) and buttressing would have occurred.

Another possible origin for the faults at La Conejera Inlet is that they were older faults reactivated during the Mesozoic extensional events and later on during the Alpine contraction.

Faults located in nearby localities with similar orientations to those of La Conejera Inlet (NE-SW striking) have been interpreted as Variscan structures inherited from the Paleozoic basement of the Cantabrian Zone (Lepvrier and Martínez-García, 1990) or formed during a Permian rifting (Martínez-García, 1981).

12.- DISCUSSION AND CONCLUSIONS

In the cliffs of La Conejera Inlet two main normal faults dipping in opposite senses crop out. The beds in the hangingwall of both faults exhibit, broadly, a double-hinge anticline of decametre-scale. Together with second order extensional structures there are a number of contractional folds and faults. These compressive elements seem to be limited to the common hangingwall of the two main faults, since only normal and strike-slip faults exist in the footwalls. The distribution of deformation along the hangingwall shows that it is progressively more intense to the NW.

In an initial extensional stage, for which we proposed a half-graben model with a detachment level situated about 50 m under the present-day topographic surface, a minimum extension of about 70-78 m would have occurred.

Later in a contractional setting, the main northern normal fault would have acted as buttress causing the concentration of deformation within its hangingwall. The shortening was consumed by buttressing, displacement over the detachment level, and reverse reactivation of the main northern fault. The total shortening has been estimated in about 20-28 m, 12 of which could be related to the reverse fault reactivation. During this mild event of positive inversion tectonics a large number of new faults (thrusts and strike-slip faults) could have been generated, together with folds, whereas some of the previous normal faults would have been cut, folded or reactivated with reverse or strike-slip components depending on their orientation respect to the stress field.

Assuming that the faults at La Conejera Inlet are the northeastern continuation of the Villaviciosa Fault, we conclude that the inversion tectonics were selective as, apparently, only some parts of the fault were affected. The displacement of the Villaviciosa Fault decreases to the NE, from about 100 m to less than 70 m. This fault also seems to change its dip along its trace, from dipping moderately to steeply to the SE (coastal cliffs), to a vertical or near vertical dip at its central sector and, finally, to the NW at its southwersternmost part. Seawards, the Villaviciosa Fault can be extended about 6 km offshore.

The main faults at La Conejera Inlet had an initial normal movement during the Middle?-Late Jurassic that could result from an extensional event corresponding to an embryonic stage of the Bay of Biscay opening, mainly from Late Jurassic to Early Cretaceous. As the opening progressed and the Iberian Plate rotated counter-clockwise, the main faults would have adopted their present-day configuration. The contraction suffered by the study area seems to have been the result of N-S shortening, coincident with the Cenozoic compression that generated the Pyrenees and its western prolongation along the N Iberian Peninsula.

13.- ACKNOWLEDGEMENTS

The authors thank the financial support by the research projects CSD2006-0041 (Geociencias en Iberia: estudios integrados de topografía y evolución 4D – TOPO-IBERIA –) and CGL2011-23628 (Desarrollo de fracturas and venas asociadas al plegamiento – FRAVEPLE –) funded by diverse Spanish Ministries. H. Uzkeda thanks the support by the Spanish Ministry of Education via an FPU gran partially funded by the European Social Fund. The journal editor, Rick Groshong and Richard Lisle are thanked for their thorough and constructive reviews, which helped to improve the manuscript.

REFERENCES

Alonso, J.L., Gallastegui, J., Garcia-Ramos, J.C., Poblet, J., 2009. Estructuras mesozoicas y cenozoicas relacionadas con la apertura y cierre parcial del Golfo de Vizcaya (Zona Cantábrica – Asturias). Guía de campo del "6º Simposio sobre el Margen Ibérico Atlántico", Oviedo.

Alonso, J.L., Pulgar, F.J., García-Ramos, J.C., Barba, P., 1996. Tertiary Basins and Alpine Tectonics in the Cantabrian Mountains, in: Friend, P.F., Dabrio, C.J. (Eds.), Tertiary basins of Spain: The stratigraphic record of crustal kinematics. Cambridge University Press, Cambridge, pp. 214-227.

Álvarez-Marrón, J., Hetzel, R., Niedennann, S., Menéndez, R., Marquínez, J., 2008. Origin, structure and exposure history of a wave-cut platform more than 1 Ma in age at the coast of northern Spain: A multiple cosmogenic nuclide approach. Geomorphology 93, 316-334.

Aurell, M., Meléndez, G., Olóriz, F. (coords.), Bádenas, B., Caracuel, J., García-Ramos, J.C., Goy, A., Linares, A., Quesada, S., Robles, S., Rodríguez-Tovar, F.J., Rosales, I., Sandoval, J., Suárez de Centi, C., Tavera, J.M., Valenzuela, M., 2002. Jurassic, in: Gibbons, W., Moreno, T. (Eds.), The Geology of Spain. Geological Society, London, pp. 213-253.

Aurell, M., Robles, S., Rosales, I., Quesada, S., Meléndez, A., Bádenas, B., García-Ramos, J.C., 2003. Transgressive/regressive cycles and Jurassic paleogeography of northeast Iberia. Sedimentary Geology 162, 239-271.

Bailey, C.M., Giorgis, S., Coiner, L., 2002. Tectonic inversion and basement buttressing: an example from the central Appalachian Blue Ridge province. Journal of Structural Geology 24, 925-936.

Barrón, E., Gómez, J.J., Goy, A., Pieren, A.P., 2006. The Triassic-Jurassic boundary in Asturias (northern Spain): Palynological characterisation and facies. Review of Palaeobotany and Palynology 138, 187-208.

Beroiz, C., Barón, A., Ramírez del Pozo, J., Giannini, G., Gervilla, M., 1972. Mapa Geológico de España, Escala 1:50.000. Hoja nº 30 (Villaviciosa). Instituto Geológico y Minero de España, Madrid.

Bradski, G., Kaehler, A., 2008. Learning OpenCV. Computer Vision with the OpenCV Library. O'Reilly Media, Sebastopol.

Comas-Rengifo, M.J., García-Martínez, J.C., Goy, A., 2010,. Sinemuriense superior en Rodiles (Asturias): biocronoestratigrafía y biohorizontes de ammonoideos, in: Ruiz-Omeñaca, J.I., Piñuela, L., García-Ramos, J.C. (Eds.), Comunicaciones del V Congreso del Jurásico de España, Museo del Jurásico de Asturias, Colunga, pp. 49-56.

Cortés, A.L., Liesa, C.L., Soria, A.R., Meléndez, A., 1999. Role of extensional structures on the location of folds and thrusts during tectonic inversion (northern Iberian Chain, Spain). Geodinamica Acta 12, 113-132.

Dart, C.J., McClay, K., Hollings, P.N., 1995. 3D analysis of inverted extensional fault systems, southern Bristol Channel basin, UK, in: Buchanan, J.G. and Buchanan, P.G. (Eds.), Basin Inversion. Geological Society Special Publications 88, pp. 393-413.

Dula, W.F., 1991. Geometric models of listric normal faults and rollover folds. AAPG Bulletin 75, 1609-1625.

Fernández-López, S., Suárez Vega, L.C., 1981. Estudio bioestratigráfico (Ammonoidea) del Aaleniense y Bajociense en Asturias. Estudios Geológicos 35, 231-239.

Fleuty, M.J., 1964. The description of folds. Proceedings of the Geologists' Association 75, 461-492.

Flor, G., 1983. Las rasas asturianas; ensayos de correlación y emplazamiento. Trabajos de Geología 13, 65-81.

Flöttmann, T., James, P., 1997. Influence of basin architecture on the style of inversion and fold-thrust belt tectonics – the southern Adelaide Fold-Thrust Belt, South Australia. Journal of Structural Geology 19, 1093-1110.

García-Mondéjar, J. ,1996. Plate reconstruction of the Bay of Biscay. Geology 24, 635-638.

García-Ramos, J.C., 1997. La sucesión jurásica de la Cuenca Asturiana: entorno paleogeográfico regional y relaciones tectónica-sedimentación. Comunicaciones del IV Congreso del Jurásico de España, Alcañiz, 13-14.

García-Ramos, J.C., Alonso, J.L., Piñuela, L., 2006. La falla de Ribadesella (Asturias): valor didáctico y patrimonial. Resúmenes de la VII Reunión de la Comisión de Patrimonio Geológico, Colunga, 19-20.

García-Ramos, J.C., Valenzuela, M., Suárez de Centi, C., 1989. Estructuras de deformación asociadas a tempestitas: ejemplos en series siliciclásticas y carbonatadas someras del Paleozoico y Jurásico de Asturias. Trabajos de Geología 18, 65-74.

Gervilla, M., Beroiz, C., Pignatelli, R., Barón, A., Coma, J.E., Felgueroso, C., Ramírez del Pozo, J., Giannini, G., 1973. Memoria del Mapa Geológico de España, escala: 1:50.000, hoja nº 30 (Villaviciosa). Instituto Geológico y Minero de España, Madrid.

Gibbs, A.D., 1983. Balanced cross-section construction from seismic sections in areas of extensional tectonics. Journal of Structural Geology 5, 153-160.

Glen, R.A., Hancock, P.L., Whittaker, A., 2006. Basin inversion by distributed deformation: the southern margin of the Bristol Channel Basin , England. Journal of Structural Geology 27, 2113-2134.

Gong, Z., Langereis, C.G., Mullender, T.A.T., 2008. The rotation of Iberia during the Aptian and the opening of the Bay of Biscay. Earth and Planetary Science Letters 273, 80-93.

Groshong, R.H., 1990. Unique determination of normal fault shape from hanging-wall bed geometry in detached half-grabens. Eclogae Geologicae Helvetiae 83, 455-471.

Groshong, R.H., 1994. Area balance, depth to detachment, and strain in extension. Tectonics 13, 1488-1497.

Gutiérrez Claverol, M., López-Fernández, C., Alonso, J.L., 2006. Procesos neotectónicos en los depósitos de rasa en la zona de Canero (Occidente de Asturias). Geogaceta 40, 75-78.

Handy, R.M., Schmid, S.M., Bousquet, R., Kissling, E., Bernoulli, D., 2010. Reconciling plate-tectonic reconstructions of Alpine Tethys with the geological-geophysical record of spreading and subduction in the Alps. Earth-Science Reviews 102, 121-156.

Hernández, J.M., 2000. Sedimentología, Paleogeografía y relación tectónica/sedimentación de los sistemas fluviales, aluviales y palustres de la cuenca rift de Aguilar (Grupo Campóo, Jurásico superior-Cretácico inferior de Palencia, Burgos, Cantabria). PhD thesis, Universidad del País Vasco-Euskal Herriko Unibertsitatea.

Knott, S.D., Beach, A., Welbon, A.I., Brockbank, P.J., 1995. Basin inversion in the Gulf of Suez: implications for exploration and development in failed rifts, in: Buchanan, J.G. and Buchanan, P.G. (Eds.), Basin Inversion. Geological Society Special Publications 88, pp. 59-81.

Lepvrier, C., Martínez-García, E., 1990. Fault development and stress evolution of the post-Hercynian Asturian basin (Asturias and Cantabria, northwestern Spain). Tectonophysics 184, 345-356.

López-Fernández, C., Pulgar, J.A., González-Cortina, J.M., Gallart, J., Díaz, J., Ruiz, M., 2004. Actividad Sísmica en el NO de la Península Ibérica observada por la red sísmica local del Proyecto GASPI. Trabajos de Geología 24, 91-106.

Malod, J.A., Mauffret, A., 1990. Iberian plate motions during the mesozoic. Tectonophysics 184, 261-278.

Martín, S., García, S., Suárez, J., Rubio, R., Gallego, R., Morán, S., 2007. VISAGE: Estereoscopio virtual aplicado a la Geología. Actas del XII Congreso Internacional de Energía y Recursos Minerales, Oviedo.

Martín, S., Uzkeda, H., Poblet, J., Bulnes, M., Rubio, R., 2013. Construction of accurate geological cross-sections along trenches, cliffs and mountain slopes using photogrammetry. Computers & Geosciences 51, 90-100.

Martínez-García, E., 1981. Tectónica y mineralizaciones pérmicas en la Cordillera Cantábrica Oriental (Noroeste de España). Cuadernos do Laboratorio Xeolóxico de Laxe 2, 263-271.

Mary, G., 1983. Evolución del margen costero de la Cordillera Cantábrica en Asturias desde el Mioceno. Trabajos de Geología 13, 3-35.

McClay, K.R., 1989: Analogue models of inversion tectonics, in: Cooper, M.A. and Williams, G.D. (Eds.), Inversion Tectonics. Geological Society Special Publications 44, pp. 41-59.

McClay, K.R., 1995: The geometries and kinematics of inverted fault systems: a review of analogue model studies, in: Buchanan, J.G. and Buchanan, P.G. (Eds.), Basin Inversion. Geological Society Special Publications 88, pp. 97-118.

Navarro Vázquez, D., Leyva Cabello, F., Rodríguez Fernández, L.R., Martínez Cienfuegos, F., Villa Otero, E., Horvath Mardones, V., Heredia Carballo, N., 1988. Cuencas carboníferas ocultas por la cobertera mesozoico-terciaria en Asturias. IGME, Madrid.

Pignatelli, R., Giannini, G., Ramírez del Pozo, J., Beroiz, C., Barón, A., 1973. Memoria y Mapa Geológico de España, escala: 1:50.000, hoja nº 15 (Lastres). Instituto Geológico y Minero de España, Madrid.

Poblet, J., Bulnes, M., 2005. Fault-slip, bed-length and area variations in experimental rollover anticlines over listric normal faults: influence in extensión and depth to detachment estimations. Tectonophysics 396, 97-117.

Poblet, J., Bulnes, M., 2007. Predicting strain using forward modelling of restored cross-sections; application to rollover anticlines over listric normal faults. Journal of Structural Geology 29, 1960-1970.

Potma, W.A., Betts, P.G., 2006. Extension-related structures in the Mitakoodi Culmination: implications for the nature and timing of extension, and effect on later shortening in the eastern Mt Isa Inlier. Australian Journal of Earth Sciences 53; 55-67.

Pujalte, V., Robles, S., García-Ramos, J.C., Hernández, J.M., 2004. El Malm-Barremiense no marinos de la Cordillera Cantábrica, in Vera, J.A. (Ed.), Geología de España. SGE-IGME, Madrid: pp. 288-291.

Pulgar, J.A., Alonso, J.L., Espina, R.G., Marín, J.A., 1999. La deformación alpina en el basamento varisco de la Zona Cantábrica. Trabajos de Geología 21, 283-294.

Quesada, S., Robles, S., 1995. Distribution of organic facies in the Liassic carbonate ramps of the Western Basque-Cantabrian (Northern Spain). Field trip guide of the 17th International Meeting on Organic Geochemistry, Donostia-San Sebastian.

Ramsay, J.G., 1967. Folding and fracturing of rocks. Mc Graw-Hill, Nueva York.

Robles, S., Pujalte, V., Hernández, J.M., Quesada, S., 1996. La sedimentación aluvio-lacustre de la Cuenca de Cires (Jurásico superior-Berriasiense de Cantabria): un modelo evolutivo de las cuencas lacustres ligadas a la etapa temprana del rift Nord-Ibérico. Cuadernos de Geología Ibérica 21, 227-251.

Robles, S., Pujalte, V., Valles, J.C., 1989. Sistemas sedimentarios del Jurásico de la parte occidental de la Cuenca Vasco-Cantábrica. Cuadernos de Geología Ibérica 13, 185-198.

Robles, S., Quesada, S., Rosales, I., Aurell, M., García-Ramos, J.C., 2004. El Jurásico marino de la Cordillera Cantábrica, in Vera, J.A. (Ed.), Geología de España. SGE-IGME, Madrid: pp. 279-285.

Rodríguez, L, Esteban, J.J., Vegas, N., Cuevas, J., 2008. Tectónica de inversión en la Playa de Sopelana (Arco Vasco, Pirineos occidentales). Geogaceta 45, 23-26.

Schöpfer, M.P.J., Childs, C., Walsh, J.J., Manzocchi, T., Koyi, H.A., 2007. Geometrical analysis of the refraction and segmentation of normal faults in periodically layered sequences. Journal of Structural Geology 29, 318-335.

Schudack, M., 1987. Charophytenflora und fazielle Entwicklung der Grenzschichten mariner Jura / Wealden in den Nordwestlichen Iberischen Ketten (mit Vergleichen zu Asturien und Kantabrien). Palaeontographica B 204, 1-80.

Schudack, M., Schudack, U., 2002. New biostratigraphical data for the Upper Jurassic of Asturias (Northern Spain) based on Ostracoda. Revista Españñola de Micropaleontología 34, 1-18.

Sibuet, J.-C., Srivastava, S.P., Spakman, W., 2004. Pyrenean orogeny and plate kinematics. Journal of Geophysical Research 109, B08104.

Suárez Rodríguez, A., 1988. Estructura del área de Villaviciosa-Libardón (Asturias, Cordillera Cantábrica). Trabajos de Geología 17, 87-98.

Suárez Vega, L.C., 1974. Estratigrafía del Jurásico de Asturias. Cuadernos de Geología Ibérica 74, 1-369.

Suppe, J., 1983. Geometry and kinematics of fault-bend folding. American Journal of Science 283, 684-721.

Uzkeda, H., Poblet, J., Bulnes, M., García-Ramos, J.C., 2010. Estructura de los materiales jurásicos en la zona de Lastres-Colunga (Asturias), in: Ruiz-Omeñaca, J.I., Piñuela, L., García-Ramos, J.C. (Eds.), Comunicaciones del V Congreso del Jurásico de España, Museo del Jurásico de Asturias, Colunga, pp. 151-152.

Valenzuela, M., García-Ramos, J.C., Suárez de Centi, C., 1986. The Jurassic sedimentation in Asturias (N Spain). Trabajos de Geología 16, 121-132.

Valenzuela, M., García-Ramos, J.C., Suárez de Centi, C.,1989. La sedimentación en una rampa carbonatada dominada por tempestades, ensayos de correlación de ciclos y eventos en la ritmita margo-calcárea del Jurásico de Asturias. Cuadernos de Geología Ibérica 13, 217-235.

Van der Voo, R., 1969. Paleomagnetic evidence for the rotation of the Iberian Peninsula. Tectonophysics 7, 5-56.

Vissers, R.L.M., Meijer, P.Th., 2012. Mesozoic rotation of Iberia: Subduction in the Pyrenees? Earth-Science Reviews 110, 93-110.

White, N., 1987. Constraints on the measurement of extension in the brittle upper crust. Norsk Geologisk Tidsskrift 67, 269-279.

White, N.J., Jackson, J.A., McKenzie, D.P., 1986. The relationship between the geometry of normal faults and that of the sedimentary layers in their hanging walls. Journal of Structural Geology 8, 897-909.

White, N.J., Yielding, G., 1991. Calculating normal fault geometries at depth: theory and examples, in Roberts, A.M., Yielding, G., Freeman, B. (Eds.), The geometry of normal faults. Geological Society Special Publications 56, pp. 251-260.

Williams, G., Vann, I., 1987. The geometry of listric normal faults and deformation in their hangingwalls. Journal of Structural Geology 9, 789-795.

Xiao, H., Suppe, J., 1992. Origin of rollover. AAPG Bulletin 76, 509-529.

Ziegler, P.A., 1988. Evolution of the Artic-North Atlantic and the Western Tethys. AAPG Memoirs 43, 1-198.

FIGURE CAPTIONS

Figure 1. a) Structural sketch of the Asturian Basin (modified from Alonso et al., 2009) indicating the location of the studied area (red dot) and b) geological map of the region close to La Conejera Inlet indicated by a red circle (simplified and modified from Beroiz et al., 1972 and Suárez Rodríguez, 1988). The location of figure 23 is shown in b).

Figure 2. Geological map of La Conejera Inlet indicating the position of the cross sections of figure 3.

Figure 3. Geological cross-section of La Conejera Inlet cliffs constructed via photogrammetric techniques. See figure 2 for location. a) Cross section including all the faults and beds interpreted on the stereoscopic pairs projected onto the selected plane. The dotted lines are the boundaries of the regions employed for the fracture intensity determination. The thick black lines correspond to the two main faults. b) Simplified and completed version of the cross section illustrated in a). c) Sketch showing the key beds employed to determine the fault displacements. The dashed lines represent the extra and interpolated portions of faults and beds.

Figure 4. Field appearance of La Conejera Inlet cliffs.

Figure 5. Equal area projections of the different sets of fractures present in the hangingwall of the main faults at La Conejera Inlet. The circles are dip-slip striae, whereas the squares

represent strike-slip ones. a) Joints, b) normal faults, some of them reactivated as left-lateral, c) reverse faults and d) right-lateral faults.

Figure 6. Geological photointerpretation of folds XII, XIV and XV (see figure 10 for their location) showing the different sets of fractures existent in the hangingwall of the main faults. Green: joints. Dark blue: normal faults. Light blue: reverse faults. Red: right-lateral faults. The right-lateral faults are approximately parallel to the outcrop surface.

Figure 7. Geological photointerpretation of anticline XVII (see location in figure 10) showing normal (dark blue) and reverse (light blue) faults that vary their dips depending on the region of the fold they are located. The equal area projections in the upper portion of the figure illustrate the normal faults, including their striae (red circles). The equal area projections in the lower part of the figure illustrate the reverse faults, including their striae (red circles).

Figure 8. Rose diagrams of the different sets of fractures to which an equal area projection of the fold axes has been superposed. a) Northwestern sector and b) southeastern sector. Green: joints. Dark blue: normal faults. Light blue: reverse faults. Red: right-lateral faults. Orange: fold axes.

Figure 9. Graphs of displacement versus distance along the fault for eight faults located in the hangingwall of the two main faults (see location in figure 10). a) F1, b) F2, c) F3, d) F4, e) F5, f) F6, g) F7 and h) F8. Solid lines: reverse faults. Dotted lines: normal faults. Dashed

lines: angle between the fault and the bedding in the northwestern fault block. Dashdot lines: angle between the fault and the bedding in the southeastern fault block.

Figure 10. Simplified geological cross-section indicating the position of folds I to XIX and faults F1 to F8, and equal area projections of the elements forming the diverse folds. Hollow circles: bedding. Solid circle: fold axes. Lines: cylindrical best-fit plane. The location of figure 20 is shown.

Figure 11. Graph showing the variation in the interlimb angle (in black) and in the amplitude to half-wavelength ratio (in light grey) versus the distance to the main northern fault for folds at the hangingwall of both main faults. The best-fit functions have been included to illustrate better the behaviour of the plotted data.

Figure 12. Geological photointerpretation of syncline XVI (see location in figure 10) displaying normal faults (dark blue) displaced by bedding (white) and by thrusts (light blue). The different stratigraphic beds have been labelled from A (oldest) to F (youngest). The equal area projection in the upper right portion of the figure illustrates the fold axis (red circle) and the bedding (hollow circles). The equal area projection in the lower left part of the figure illustrates bedding surfaces containing flexural-slip striae (red circles).

Figure 13. a) π diagram of the northwestern sector bedding, including the best-fit plane and b) π diagram of the southeastern sector bedding, including the best-fit plane.

Figure 14. Geological photointerpretation of the fault-related anticline XIX (see location in figure 10).

Figure 15. Rose diagram showing the different sets of fractures identified in the footwalls of the main faults. Green: joints. Dark blue: normal faults. Red: right-lateral faults.

Figure 16. Equal area projection of the sets of fractures present in the footwall of the main faults. The circles are dip-slip (approximately pure) striae, whereas the squares represent strike-slip ones. a) Joints, b) normal faults, some of them reactivated as left-lateral, and c) right-lateral faults.

Figure 17. Geological photointerpretation showing two conjugate faults in the footwall of the main northern fault.

Figure 18. Geological photointerpretation of a bedding surface showing the sets of fractures existent in the footwall of the main northern fault. Green: joints. Dark blue: normal faults. Red: right-lateral faults.

Figure 19. End member interpretations for the extensional geometry of the structure developed at La Conejera Inlet: a) half-graben and b) asymmetric graben.

Figure 20. a) Photography of the immediacies of the main northern fault showing the intense deformation present and b) geological photointerpretation. The main fault is shown with a thicker line.

Figure 21. Sketch showing the two different possibilities for the geometry of the structures at La Conejera Inlet during the compression taking the half-graben hypothesis as starting point: a) buckling, and b) buckling + bending.

Figure 22. Idealized structural sketch of La Conejera Inlet showing the different types of faults and the possible orientation of the compressive tectonic transport vector deduced from the structures present.

Figure 23. Simplified structural sketch and schematic cross-sections showing the different orientations of the Villaviciosa Fault. See location in figure 1. Map simplified and modified from Beroiz et al. (1972) and Suárez Rodríguez (1988); cross sections simplified and modified from Beroiz et al. (1972) (B-B' section), Suárez Rodríguez (1988) (A-A' and C-C' sections) and Pulgar et al. (1999) (D-D' section).

Figure 24. a) Bathymetry of the area to the NE of La Conejera Inlet. Bathymetric lines interval of 10 m. b) Slope map. Both maps were constructed using data provided by the Hydrographic Institute of the Spanish Navy.

Figure 25. Comparison of the stratigraphic series of the Rodiles Formation in the localities of Santa Mera and Rodiles. Data taken from Suárez Vega (1974). The white lines indicate the location of the stratigraphic sections.

Figure 26. Possible evolutive models of La Conejera Inlet main northern fault with respect to the sedimentation of the Rodiles Formation. a) Pre-tectonic, b) syntectonic and c) post-tectonic deposition. The arrows indicate when the fault is active. The labels indicate the stratigraphic unit deposited at each time interval. The scale is approximated.

Figure 27. Equal area projection of the fold axes (circles), striae (squares for normal faults, triangles for reverse ones) and cross section planes (black: northwestern sector, light grey: southeastern sector).

Figure 28. Synthetic geological cross-section of the cliffs at La Conejera Inlet with the detachment levels calculated employing different methods. Orange: bed-length preservation method (Gibbs, 1983). Light green: heave method (Gibbs, 1983). Purple: antithetic shear method (White, 1987). Pink: displacement along the fault plane method (Williams and Vann, 1987). Blue: lost-area method (Groshong, 1994). Red: fault-bend fold “method” (Suppe, 1983). Dark green: area balance.

Figure 29. Graph obtained applying the Groshong (1994) method to estimate the detachment depth. The reference elevation is the detachment depth estimated through the fault-bend fold method.

Figure 30. Graphs obtained applying the Poblet and Bulnes (2005a) technique to estimate the detachment depth using data from the following methods: antithetic shear (solid line), heave (dotted line) and bed length (dashed line).

Figure 31. Extension and shortening estimations. a) Remaining extension, b) reverse reactivation, c) shortening estimated by bed-length preservation and d) shortening estimated by area balance.

Figure 32. Idealized sketches showing the possible evolution of the structures at La Conejera Inlet in relation with the Iberian Plate movements. a) Situation during the Late Jurassic after the

generation of La Conejera main faults, in a embryonic stage of the Bay of Biscay opening (modified from Vissers and Meijer, 2012); b) situation in the Late Cretaceous after the largest rotation of the Iberian Plate and opening of the Bay of Biscay (modified from Vissers and Meijer, 2012); c) situation in the Cenozoic after the Alpine compression responsible for the formation of the Pyrenees and its western prolongation.

TABLE CAPTIONS

Table 1: summary of the main elements of the folds analyzed. d: measured in the field or on the constructed geological cross-section. When no specified, the values were calculated via equal area projection of the bedding orientations. *: measured on the geological cross-section. **: distance from the fold hinge to the main northern fault (measured from the lowest vertex of the fault in the three-dimensional interpretation).

Table 2: fault displacements, extension and shortening of the main faults at La Conejera Inlet. The sentences in brackets indicate the procedures employed to estimate the values.

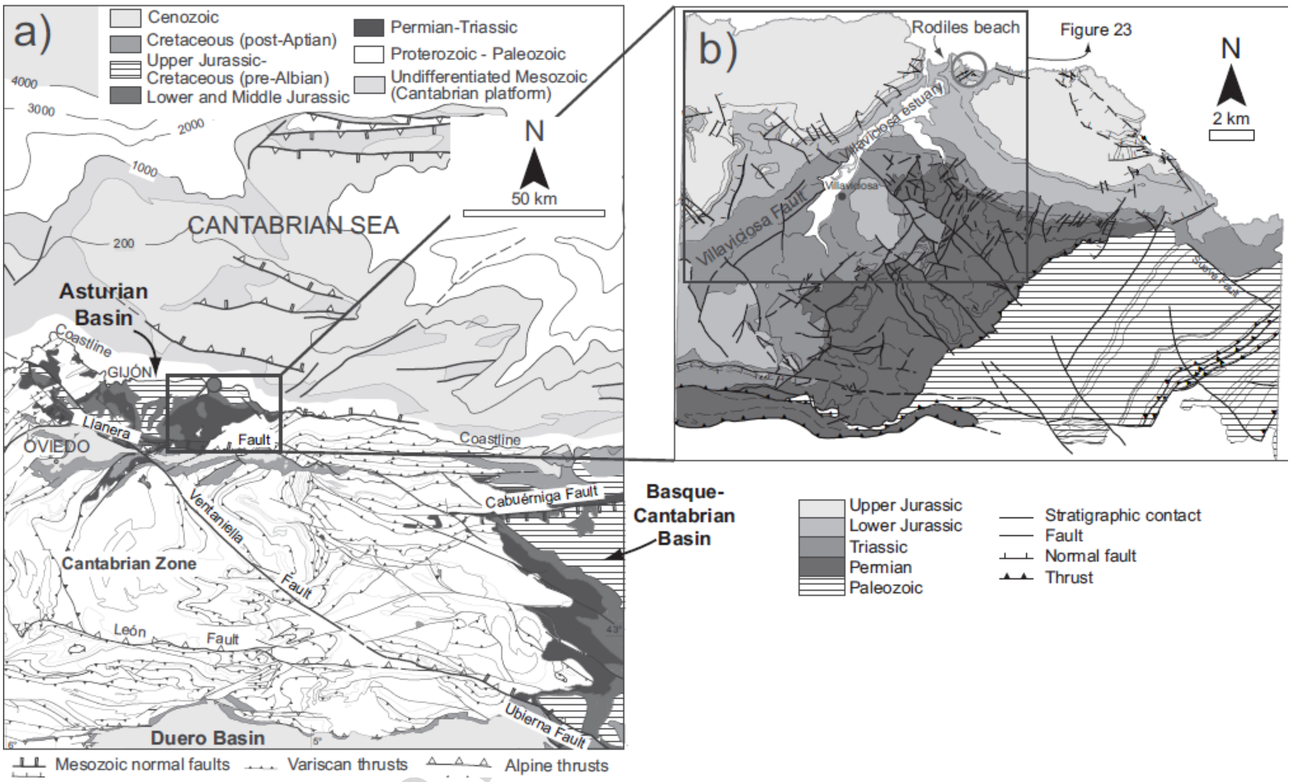
a)
Cenozoic
Cretaceous (post-Aptian)
Upper Jurassic-Cretaceous (pre-Albian)
Lower and Middle Jurassic
Permian-Triassic
Proterozoic - Paleozoic
Undifferentiated Mesozoic (Cantabrian platform)
4000
3000
2000
1000
200
N
50 km
CANTABRIAN SEA
Asturian Basin
Coastline
GIJÓN
Llanera Fault
OVIEDO
Coastline
Cabuérniga Fault
Basque-Cantabrian Basin
Ventaniella Fault
Cantabrian Zone
León Fault
Duero Basin
Ubierna Fault
Mesozoic normal faults
Variscan thrusts
Alpine thrusts
b)
Rodiles beach
Figure 23
N
2 km
Villaviciosa estuary
Villaviciosa
Villaviciosa Fault
Sueve Fault
Upper Jurassic
Lower Jurassic
Triassic
Permian
Paleozoic
Stratigraphic contact
Fault
Normal fault
Thrust

Fig. 1

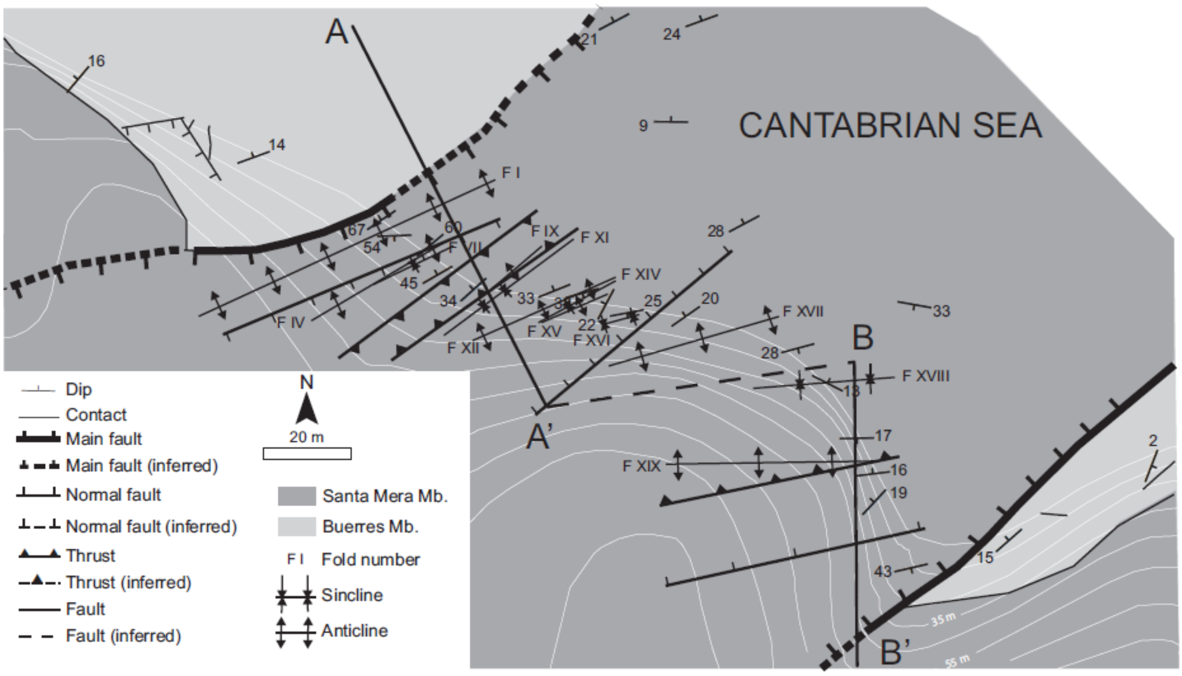
A
B
A'
B'
CANTABRIAN SEA
16
14
21
24
9
67
54
60
45
34
33
3?
22
25
20
28
28
33
13
17
16
19
43
15
2
F I
F IV
F VII
F IX
F XI
F XII
F XIV
F XV
F XVI
F XVII
F XVIII
F XIX
35 m
55 m
Dip
Contact
Main fault
Main fault (inferred)
Normal fault
Normal fault (inferred)
Thrust
Thrust (inferred)
Fault
Fault (inferred)
N
20 m
Santa Mera Mb.
Buerres Mb.
F I Fold number
Sincline
Anticline

Fig. 2

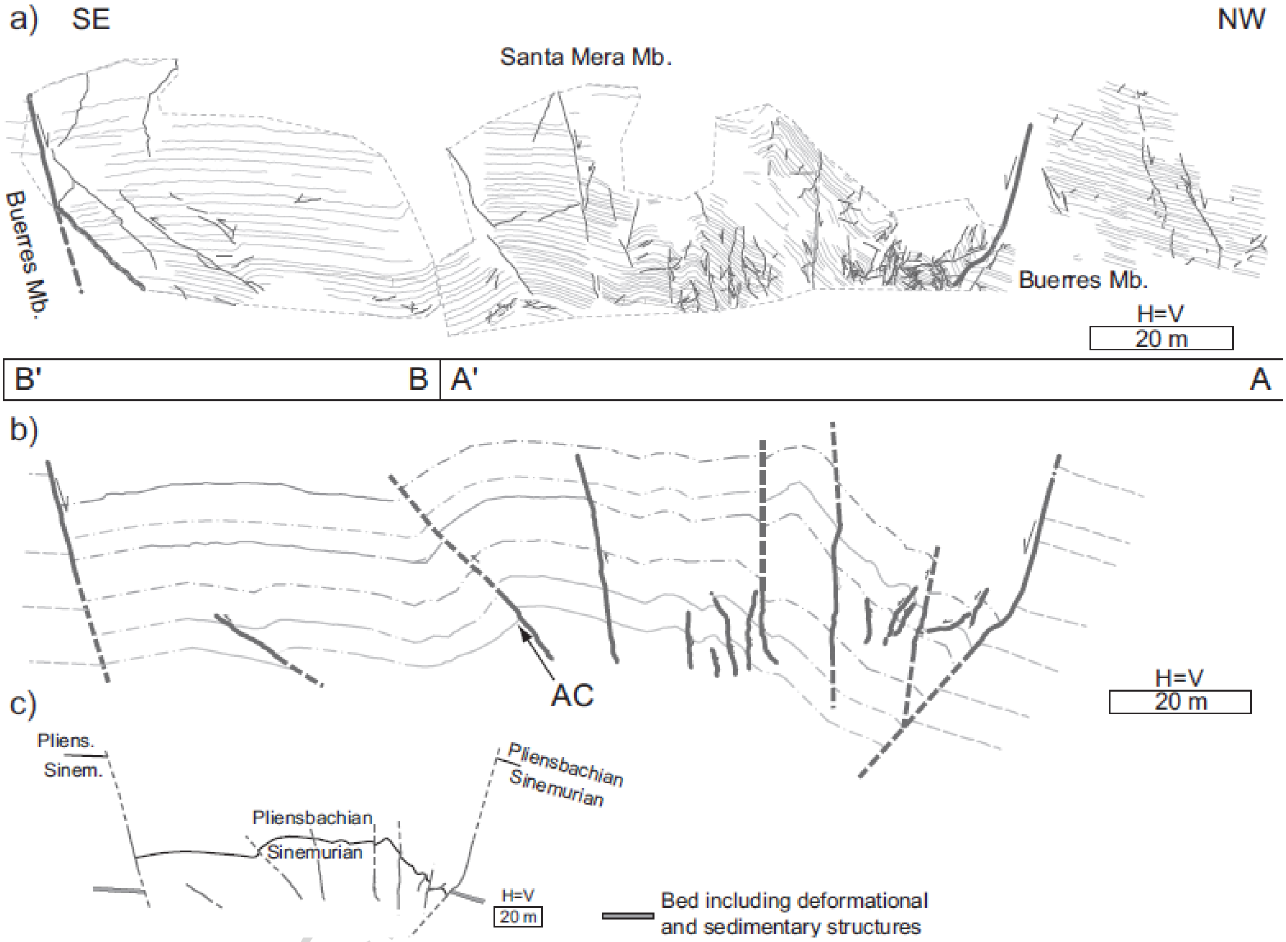
a)
SE
NW
Santa Mera Mb.
Buerres Mb.
Buerres Mb.
H=V
20 m
B'
B
A'
A
b)
AC
H=V
20 m
c)
Pliens.
Sinem.
Pliensbachian
Sinemurian
Pliensbachian
Sinemurian
H=V
20 m
Bed including deformational and sedimentary structures

Fig. 3

Fig. 4

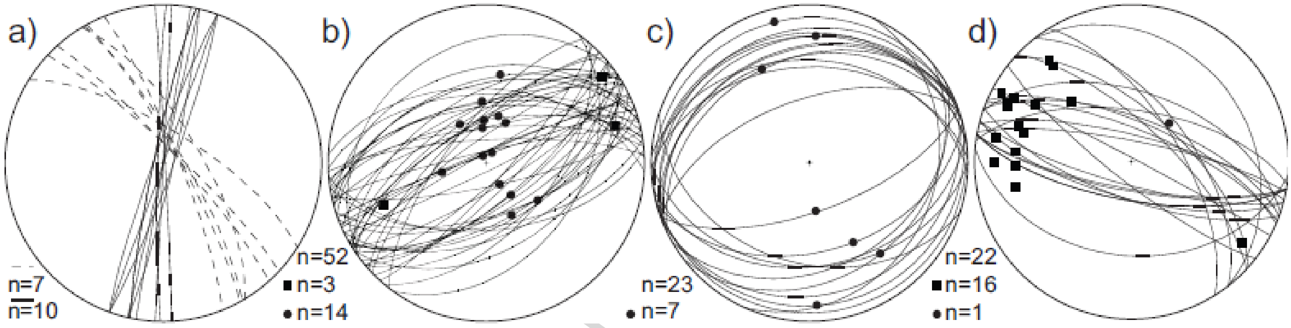

Fig. 5

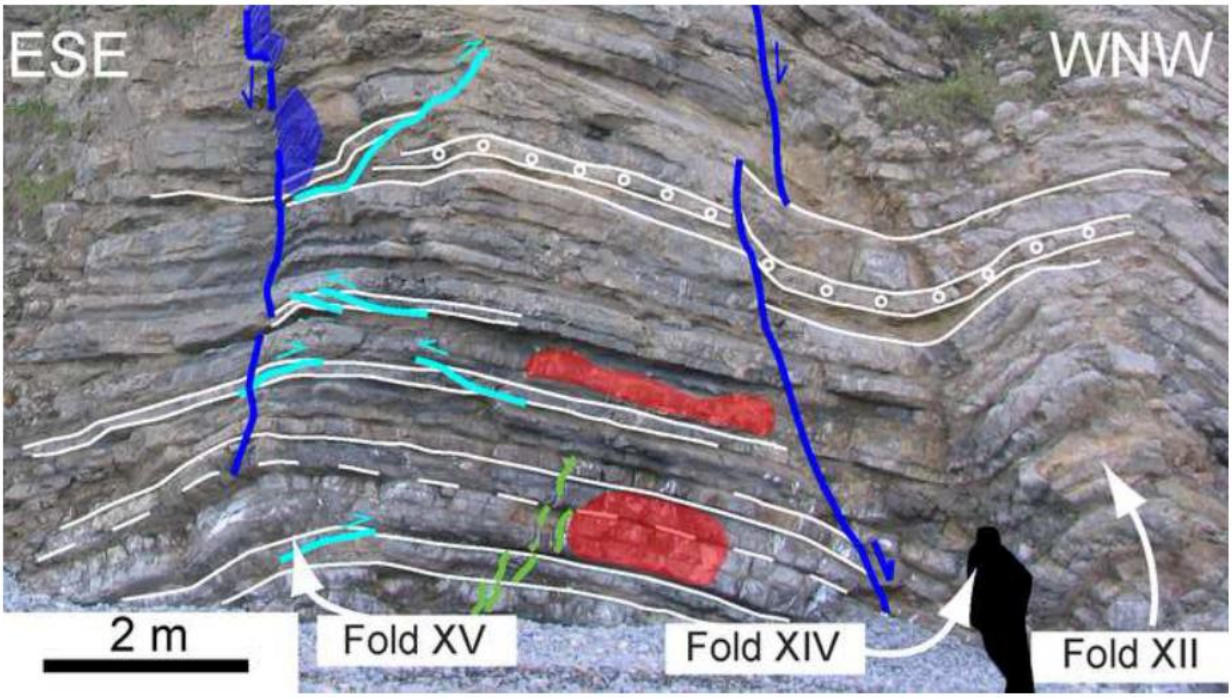

Fig. 6

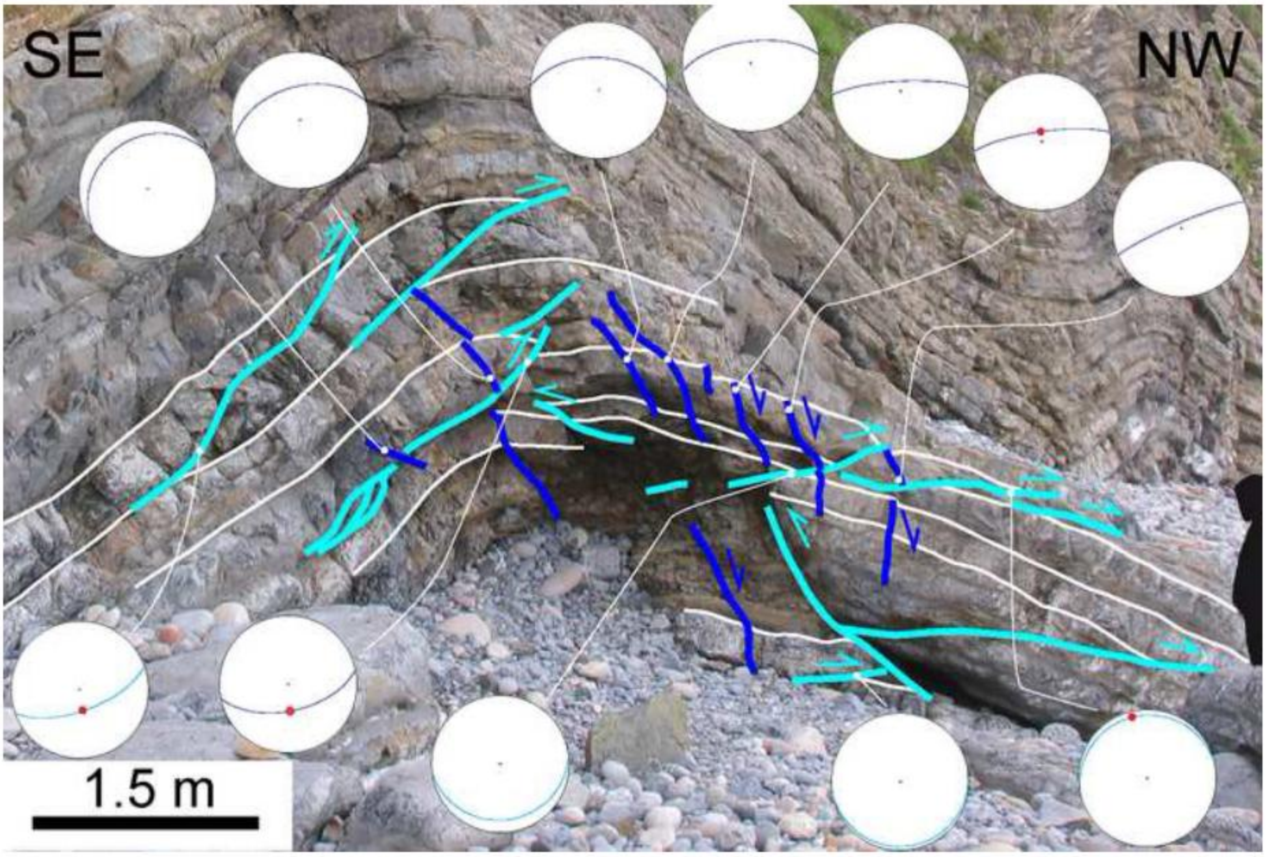

Fig. 7

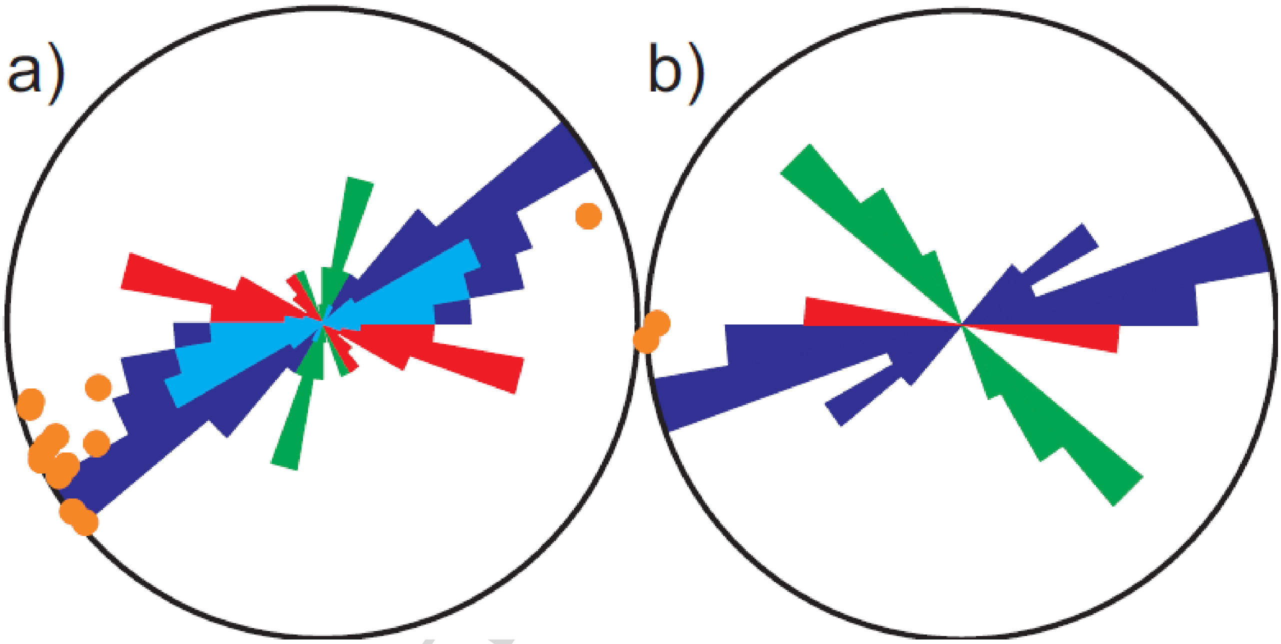

Fig. 8

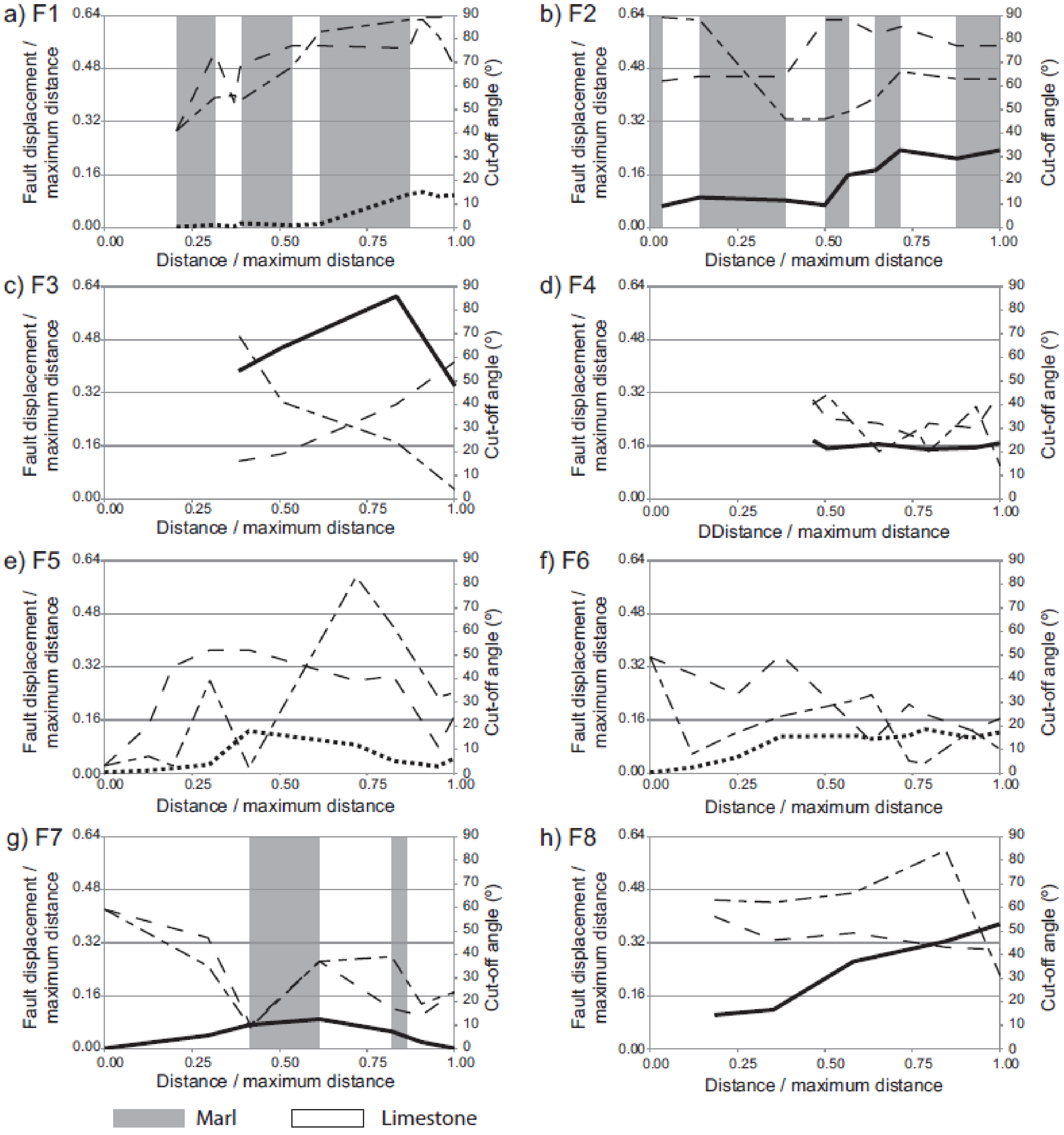
a) F1
b) F2
c) F3
d) F4
e) F5
f) F6
g) F7
h) F8
Fault displacement / maximum distance
Cut-off angle (°)
Distance / maximum distance
DDistance / maximum distance
0.00
0.16
0.32
0.48
0.64
0.25
0.50
0.75
1.00
0
10
20
30
40
50
60
70
80
90
Marl
Limestone

Fig. 9

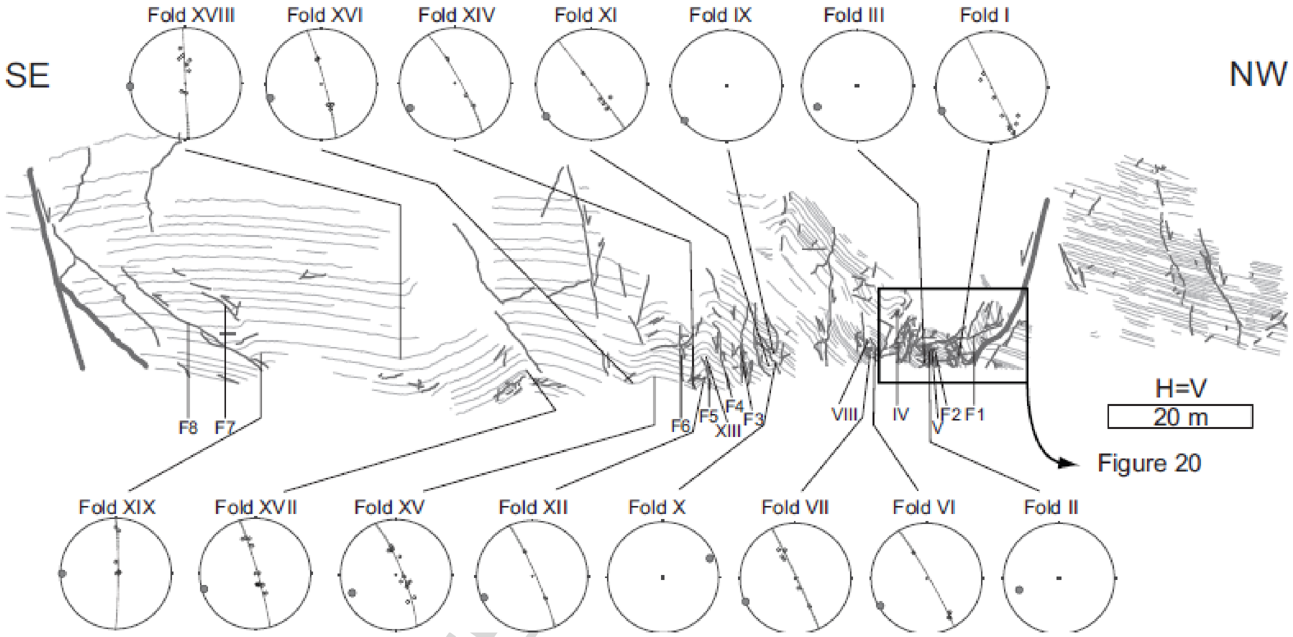
SE
NW
Fold XVIII
Fold XVI
Fold XIV
Fold XI
Fold IX
Fold III
Fold I
F8
F7
F6
F5
F4
XIII
F3
VIII
IV
V
F2
F1
H=V
20 m
Figure 20
Fold XIX
Fold XVII
Fold XV
Fold XII
Fold X
Fold VII
Fold VI
Fold II

Fig. 10

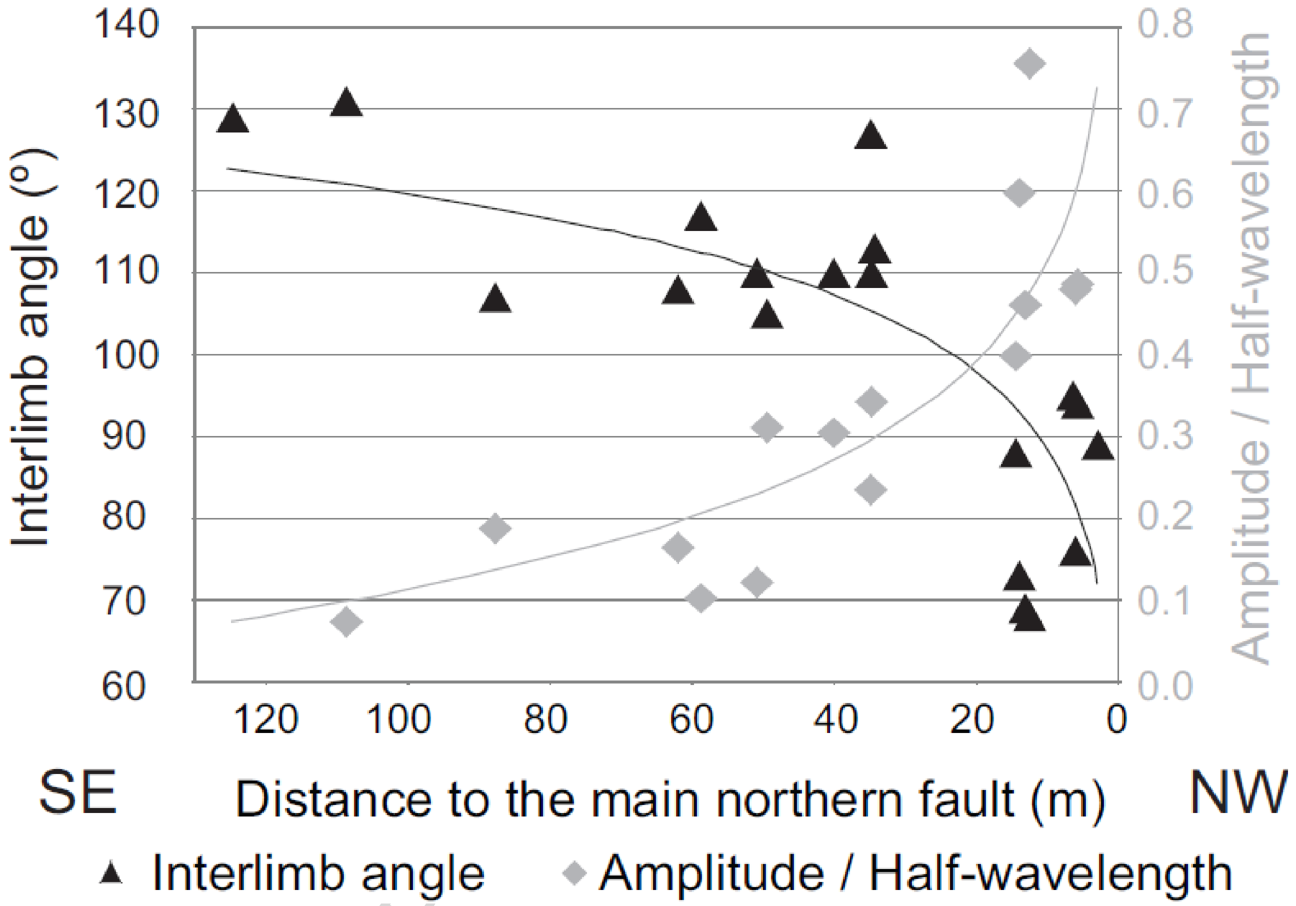
140
130
120
110
100
90
80
70
60
Interlimb angle (°)
0.8
0.7
0.6
0.5
0.4
0.3
0.2
0.1
0.0
Amplitude / Half-wavelength
120
100
80
60
40
20
0
SE
Distance to the main northern fault (m)
NW
▲ Interlimb angle
◆ Amplitude / Half-wavelength

Fig. 11

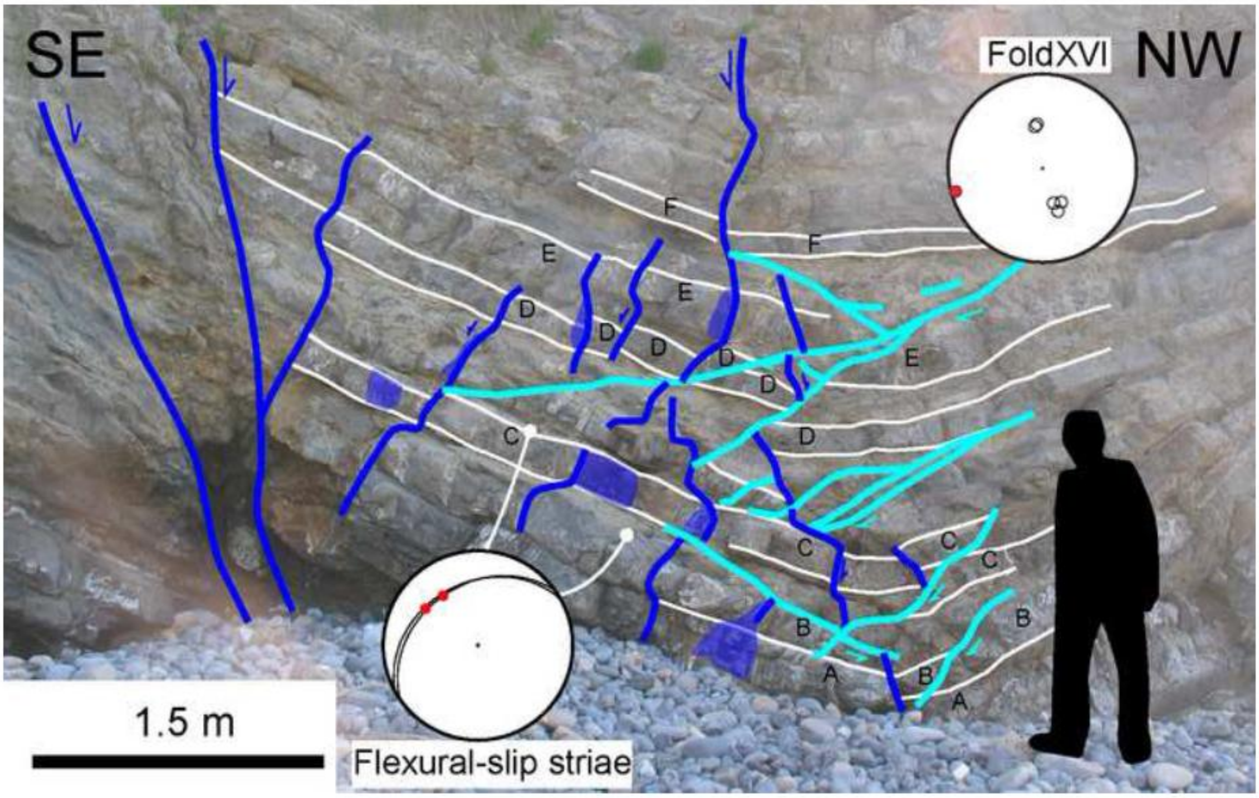
SE
NW
FoldXVI
F
F
E
E
E
D
D
D
D
D
D
C
C
C
C
B
B
B
A
A
1.5 m
Flexural-slip striae

Fig. 12

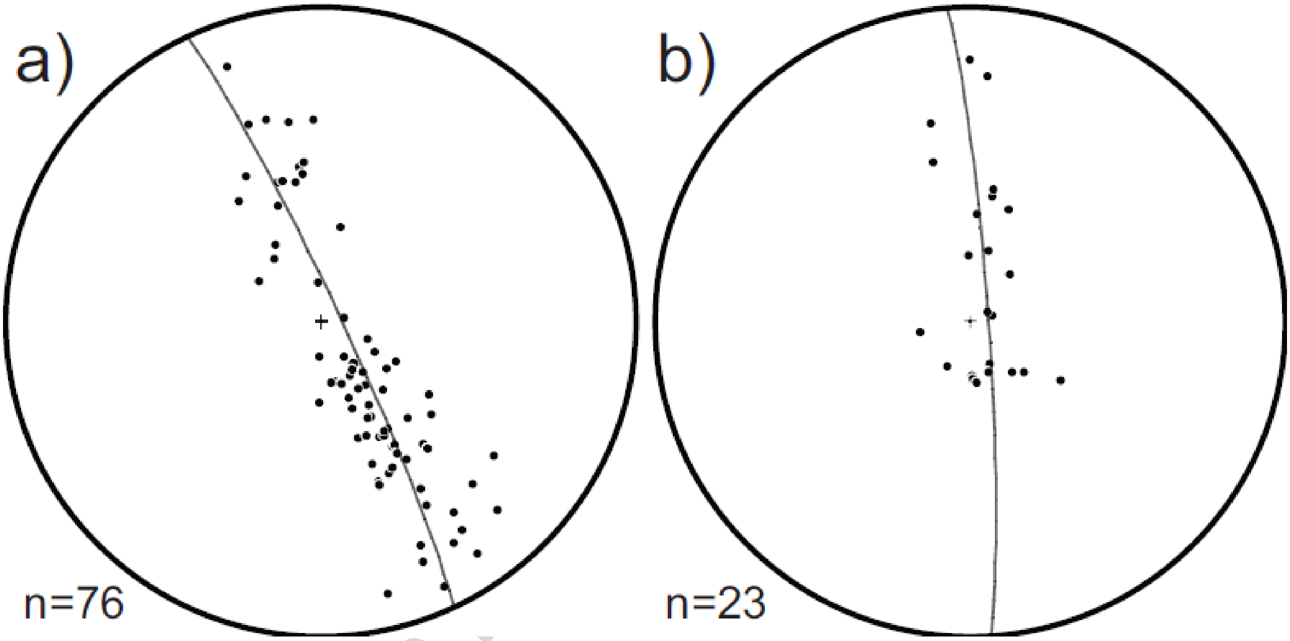

Fig. 13

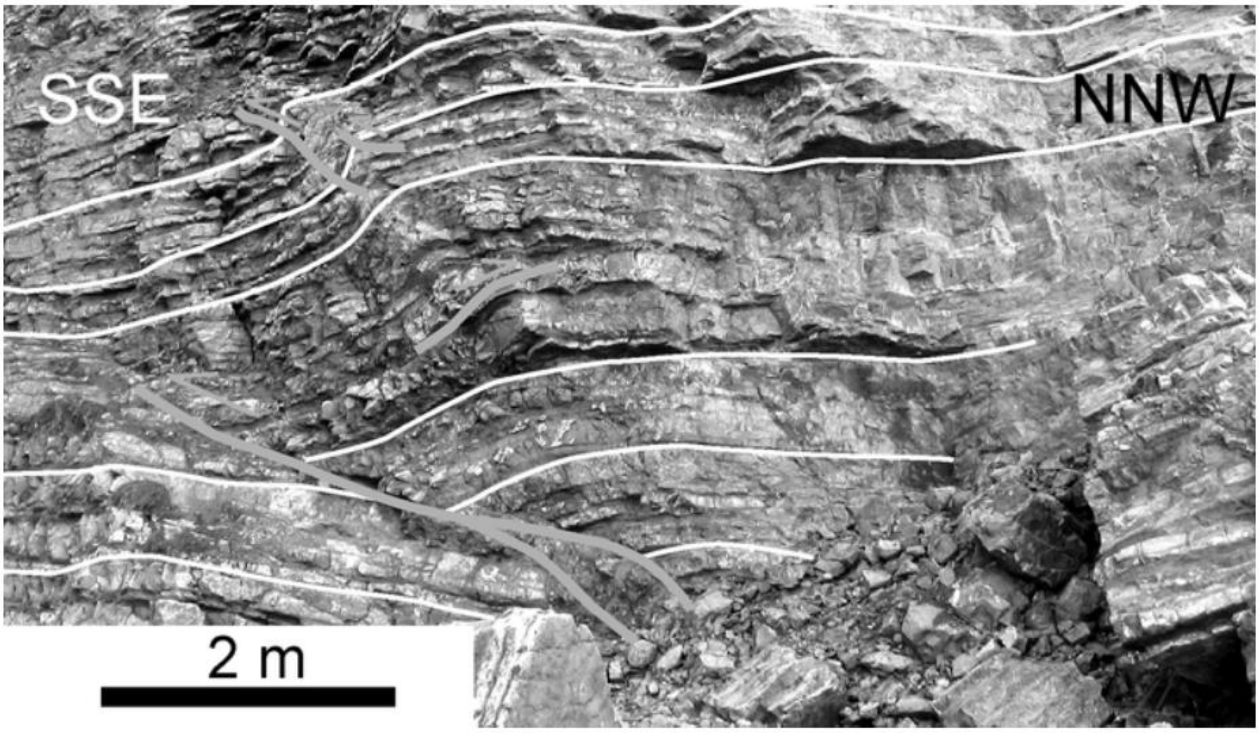

Fig. 14

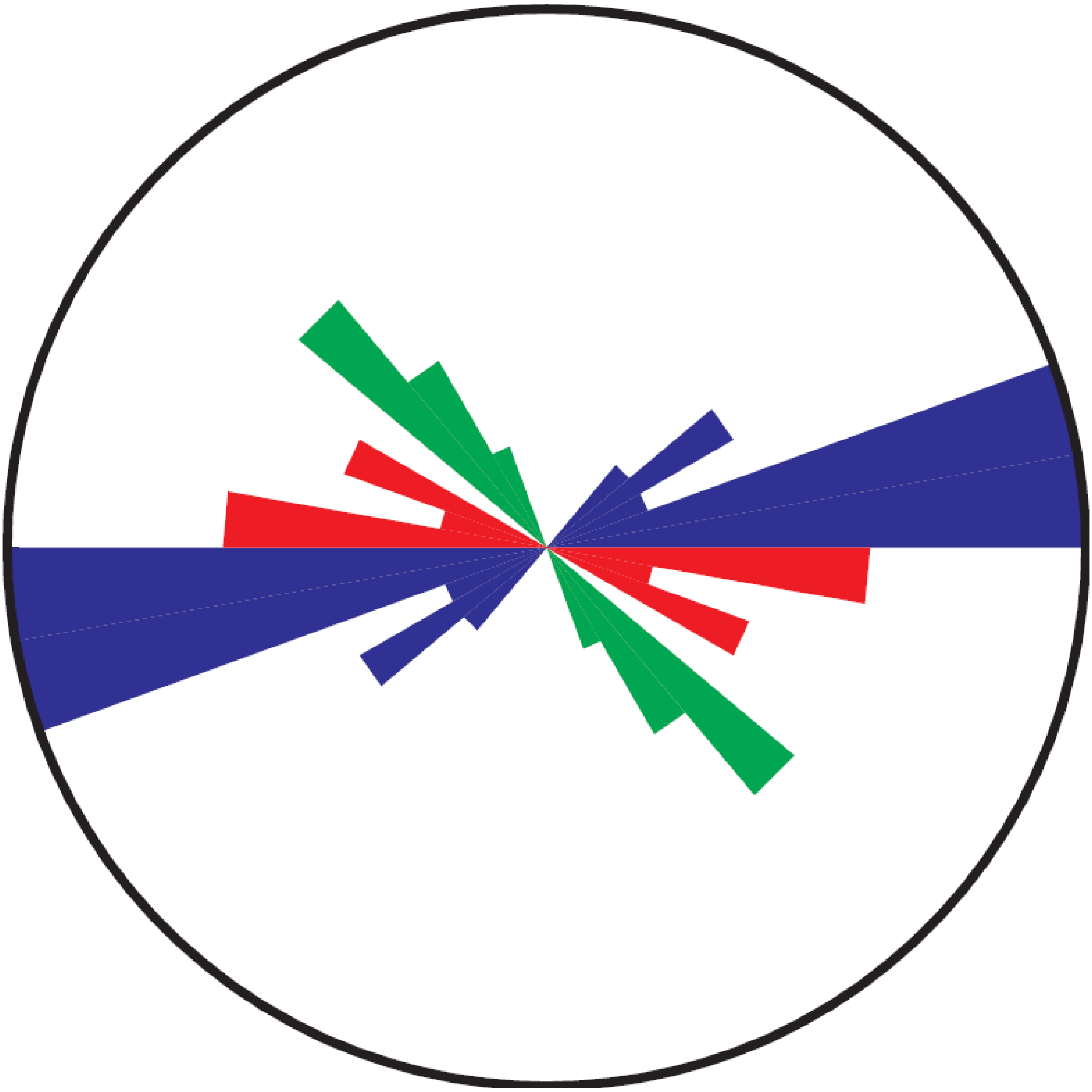

Fig. 15

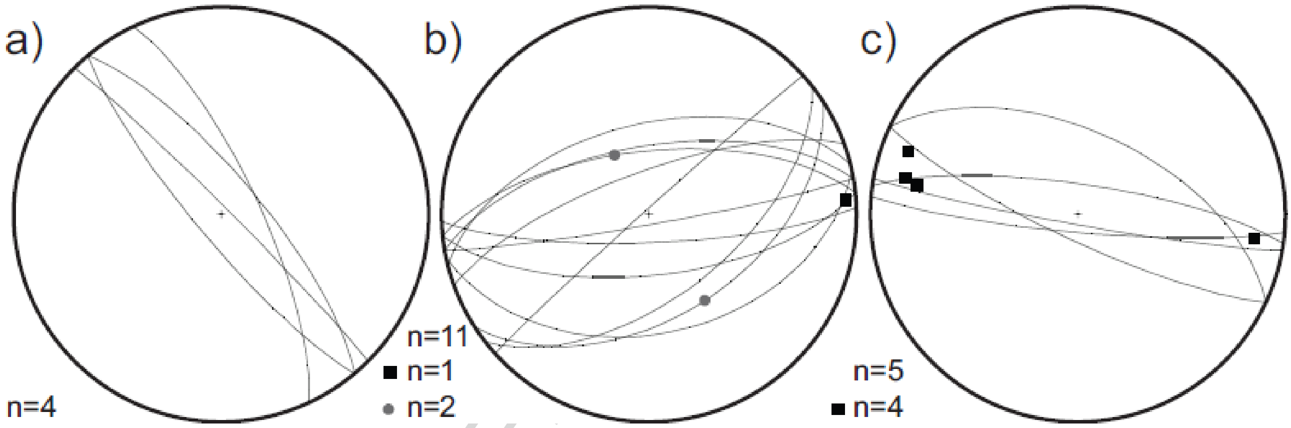

Fig. 16

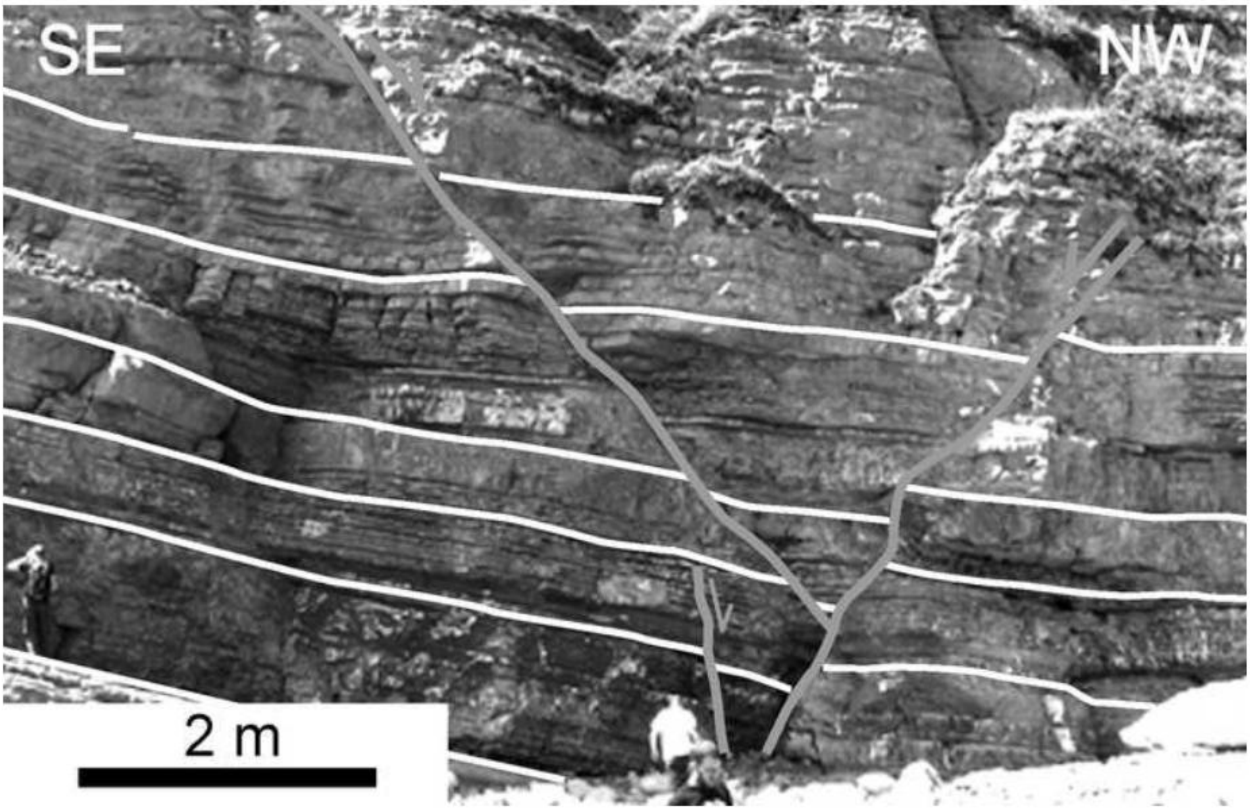

Fig. 17

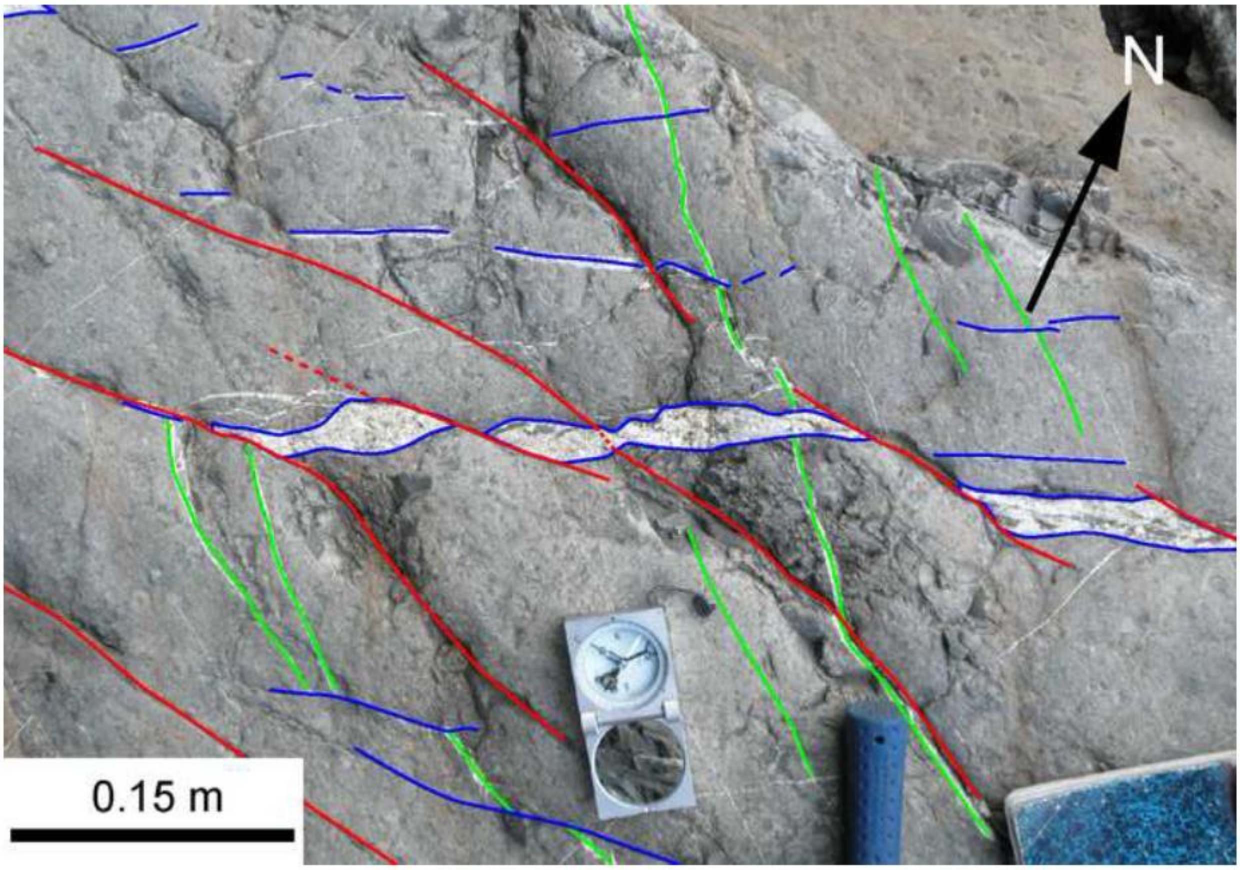

Fig. 18

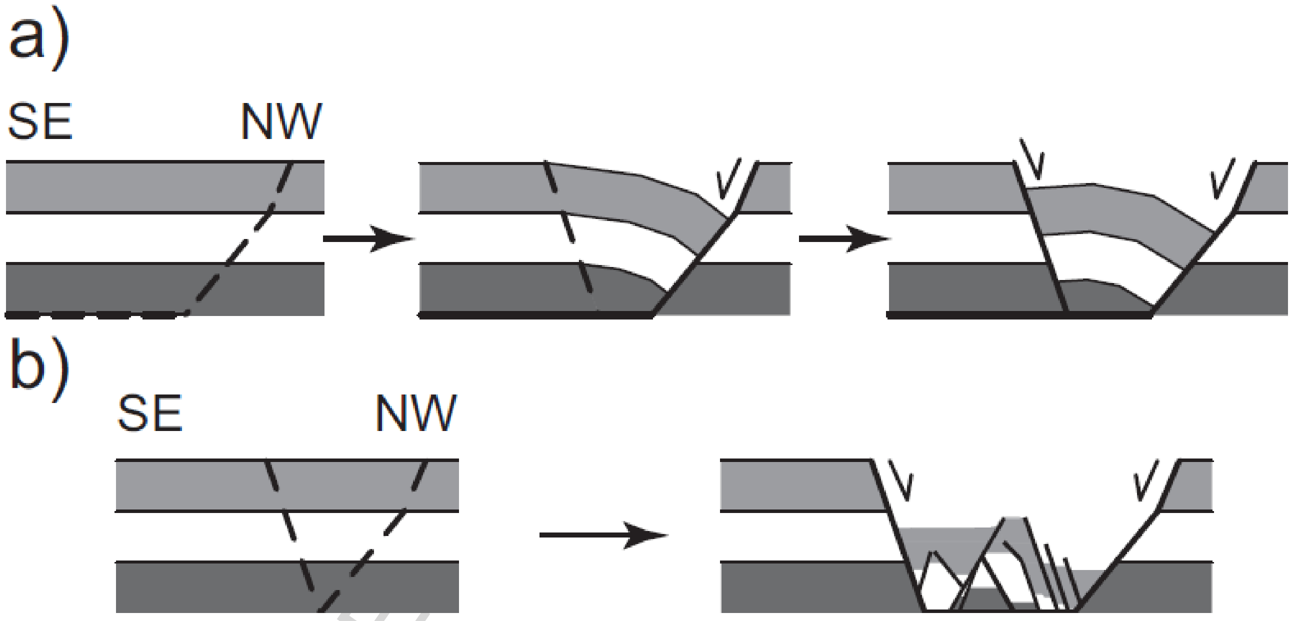

Fig. 19

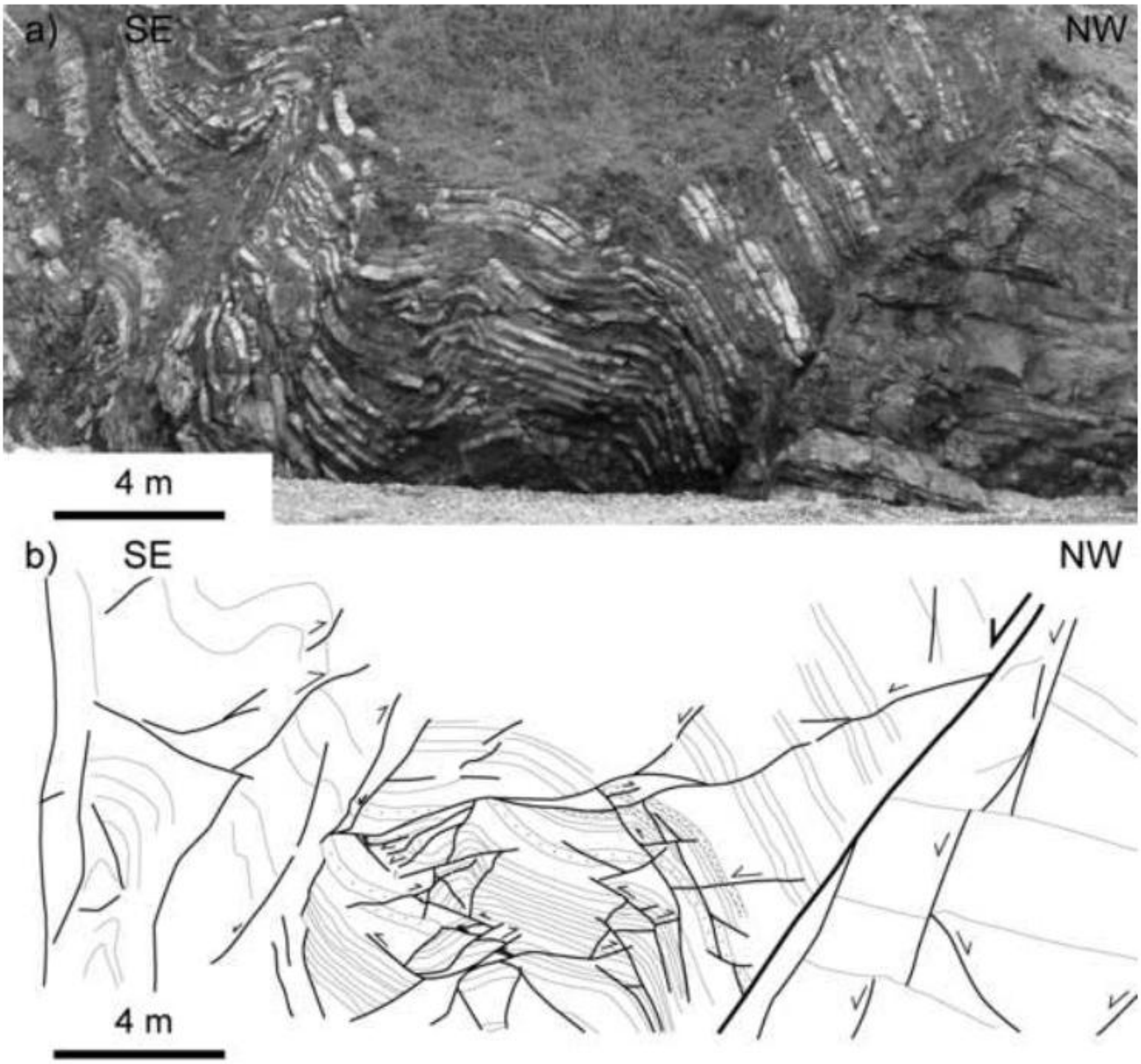

Fig. 20

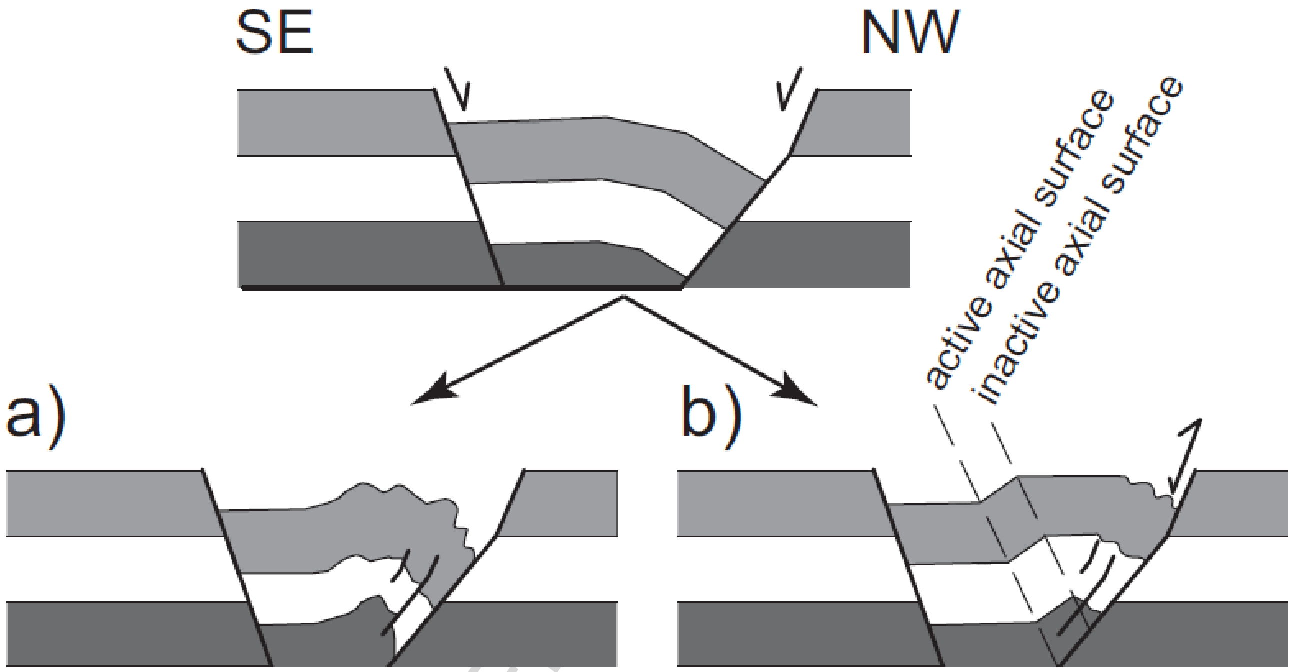

Fig. 21

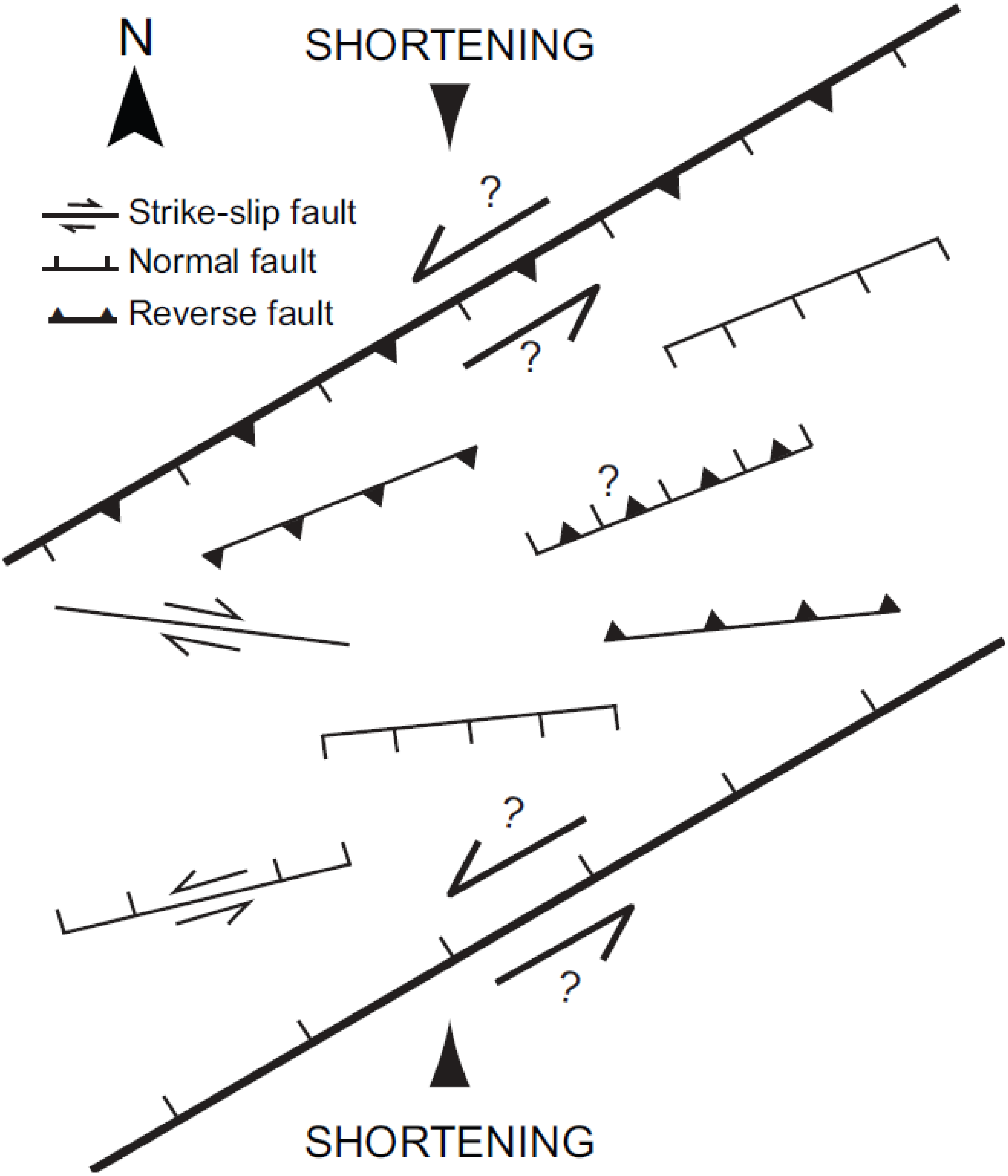
N
SHORTENING
Strike-slip fault
Normal fault
Reverse fault
?
?
?
?
?
SHORTENING

Fig. 22

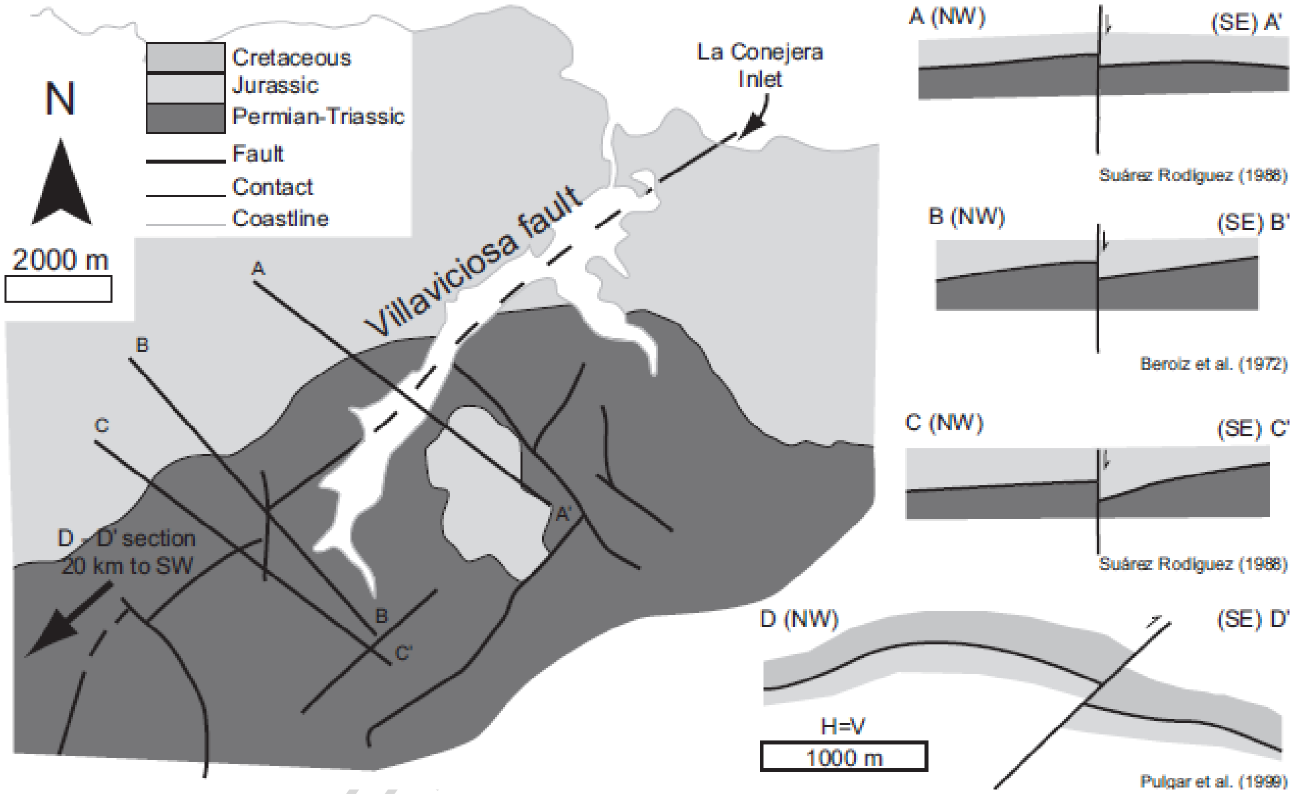
N
2000 m
Cretaceous
Jurassic
Permian-Triassic
Fault
Contact
Coastline
La Conejera Inlet
Villaviciosa fault
A
B
C
A'
B
C'
D - D' section 20 km to SW
A (NW)
(SE) A'
Suárez Rodíguez (1988)
B (NW)
(SE) B'
Beroiz et al. (1972)
C (NW)
(SE) C'
Suárez Rodíguez (1988)
D (NW)
(SE) D'
H=V
1000 m
Pulgar et al. (1999)

Fig. 23

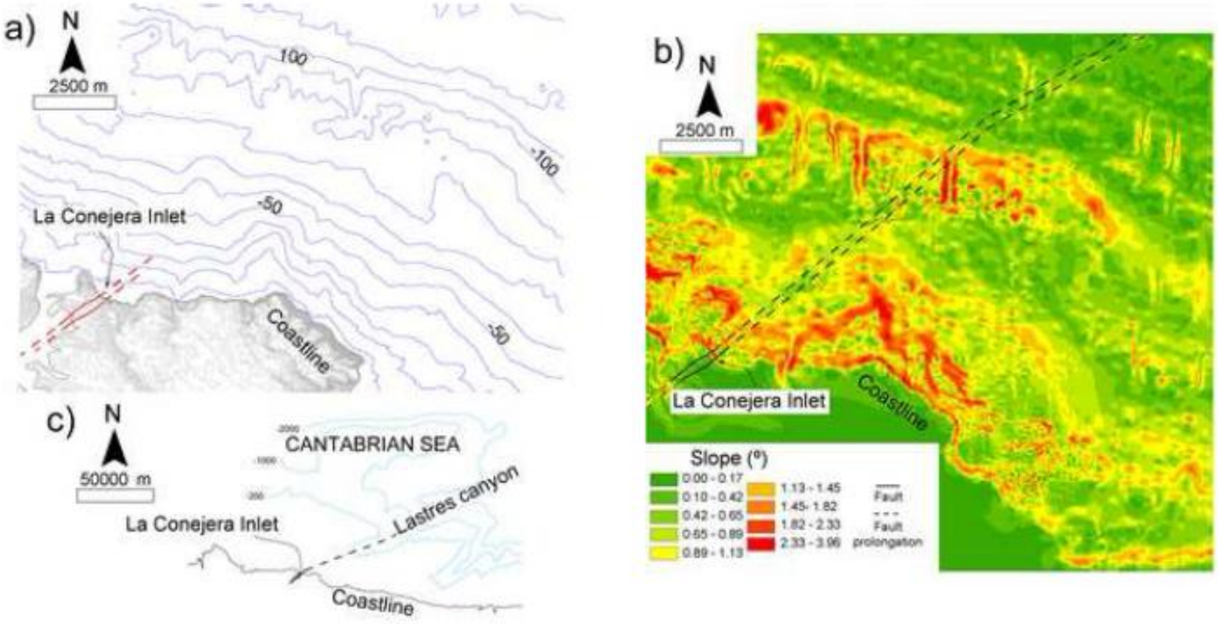
a)
N
2500 m
100
-100
-50
La Conejera Inlet
Coastline
-50
b)
N
2500 m
La Conejera Inlet
Coastline
Slope (°)
0.00 - 0.17
0.10 - 0.42
0.42 - 0.65
0.65 - 0.89
0.89 - 1.13
1.13 - 1.45
1.45- 1.82
1.82 - 2.33
2.33 - 3.96
Fault
Fault prolongation
c)
N
50000 m
CANTABRIAN SEA
-2000
-1000
-200
Lastres canyon
La Conejera Inlet
Coastline

Fig. 24

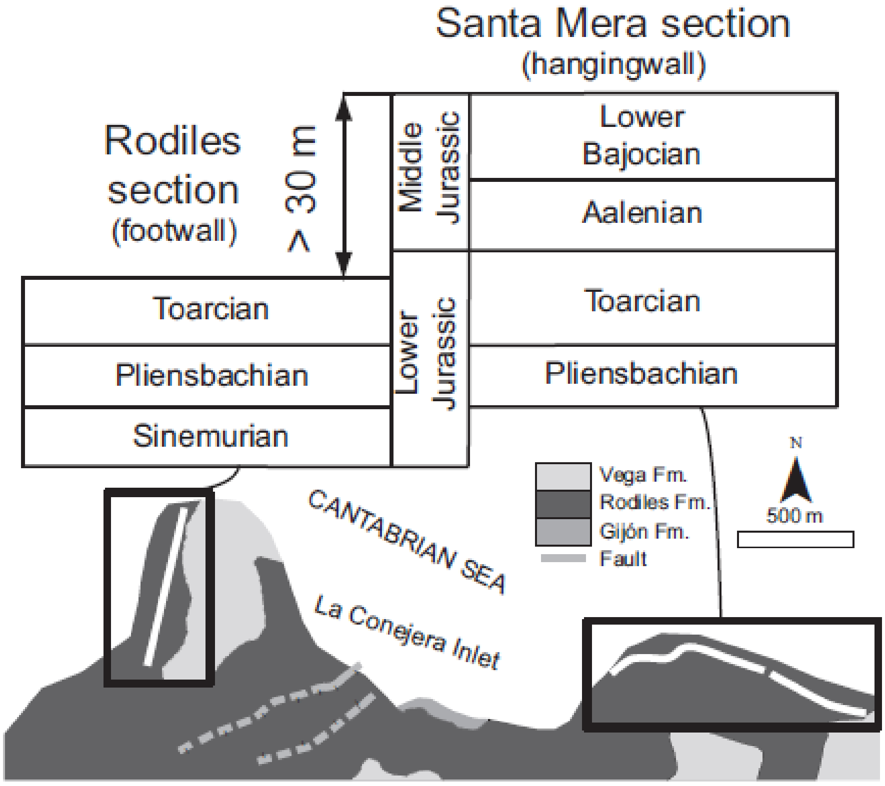
Santa Mera section
(hangingwall)
Rodiles section
(footwall)
> 30 m
Middle Jurassic
Lower Jurassic
Lower Bajocian
Aalenian
Toarcian
Pliensbachian
Toarcian
Pliensbachian
Sinemurian
CANTABRIAN SEA
La Conejera Inlet
Vega Fm.
Rodiles Fm.
Gijón Fm.
Fault
N
500 m

Fig. 25

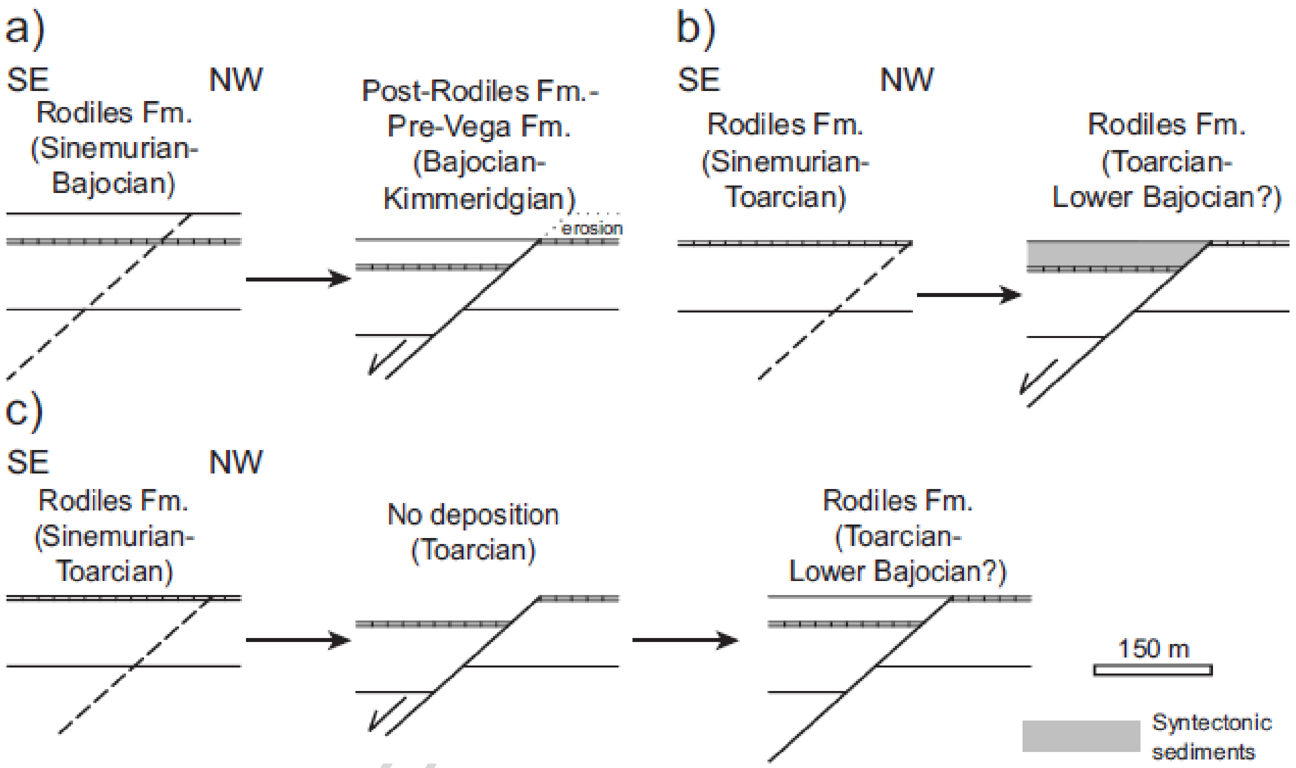
a)
SE
NW
Rodiles Fm.
(Sinemurian-
Bajocian)
Post-Rodiles Fm.-
Pre-Vega Fm.
(Bajocian-
Kimmeridgian)
erosion
b)
SE
NW
Rodiles Fm.
(Sinemurian-
Toarcian)
Rodiles Fm.
(Toarcian-
Lower Bajocian?)
c)
SE
NW
Rodiles Fm.
(Sinemurian-
Toarcian)
No deposition
(Toarcian)
Rodiles Fm.
(Toarcian-
Lower Bajocian?)
150 m
Syntectonic
sediments

Fig. 26

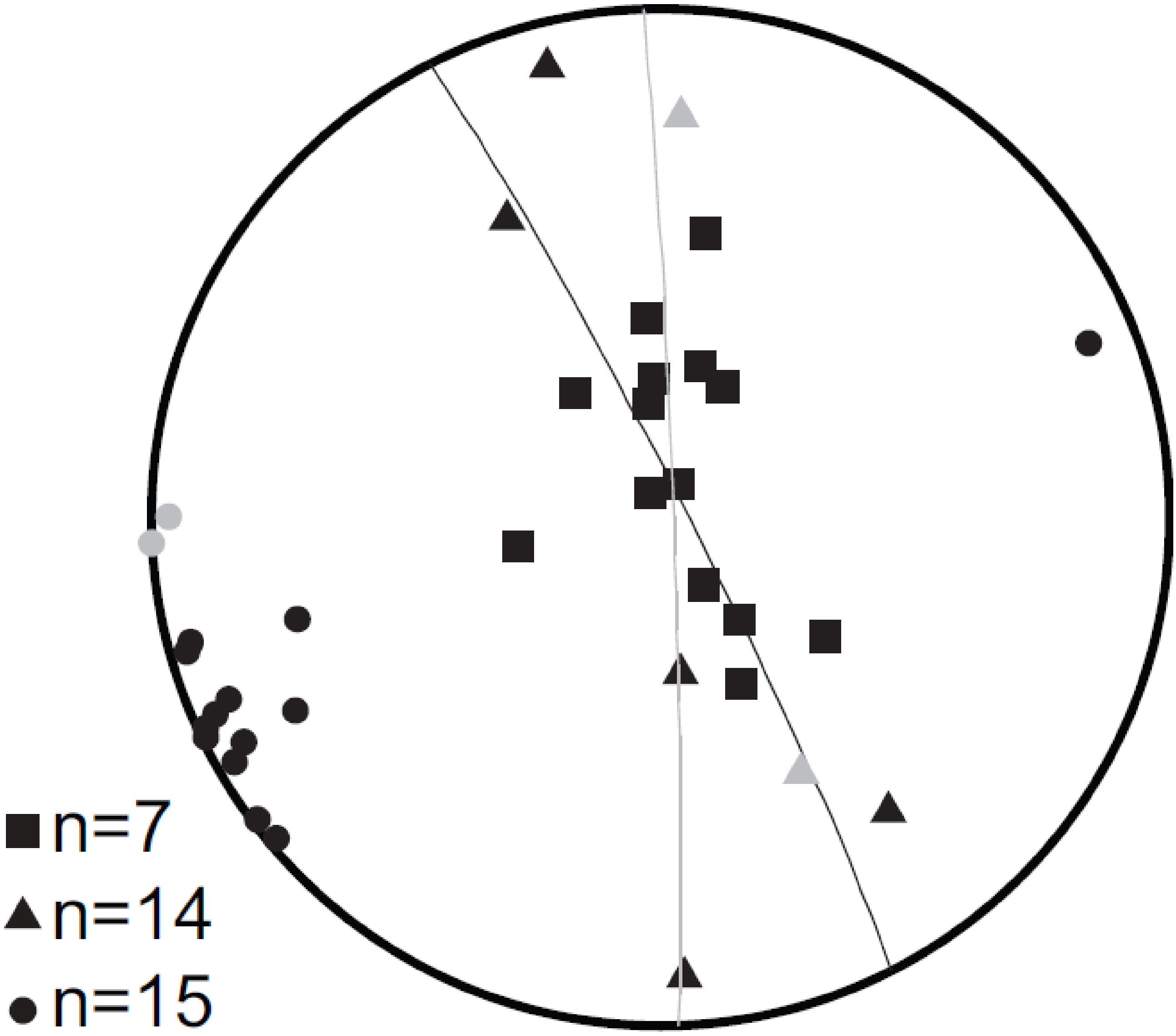

Fig. 27

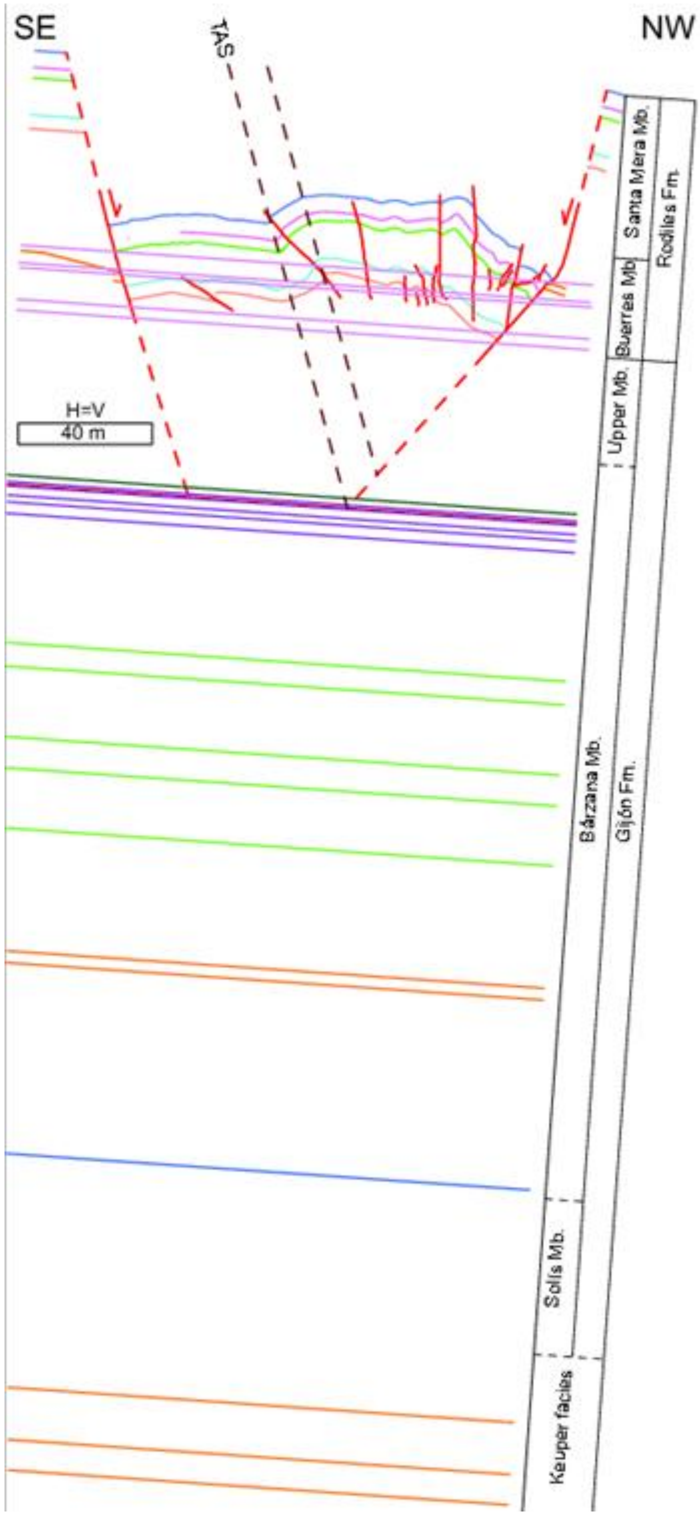
SE
TAS
NW
Santa Mera Mb.
Rodiles Fm.
Buerres Mb.
Upper Mb.
H=V
40 m
Bárzana Mb.
Gijón Fm.
Solís Mb.
Keuper facies

Fig. 28

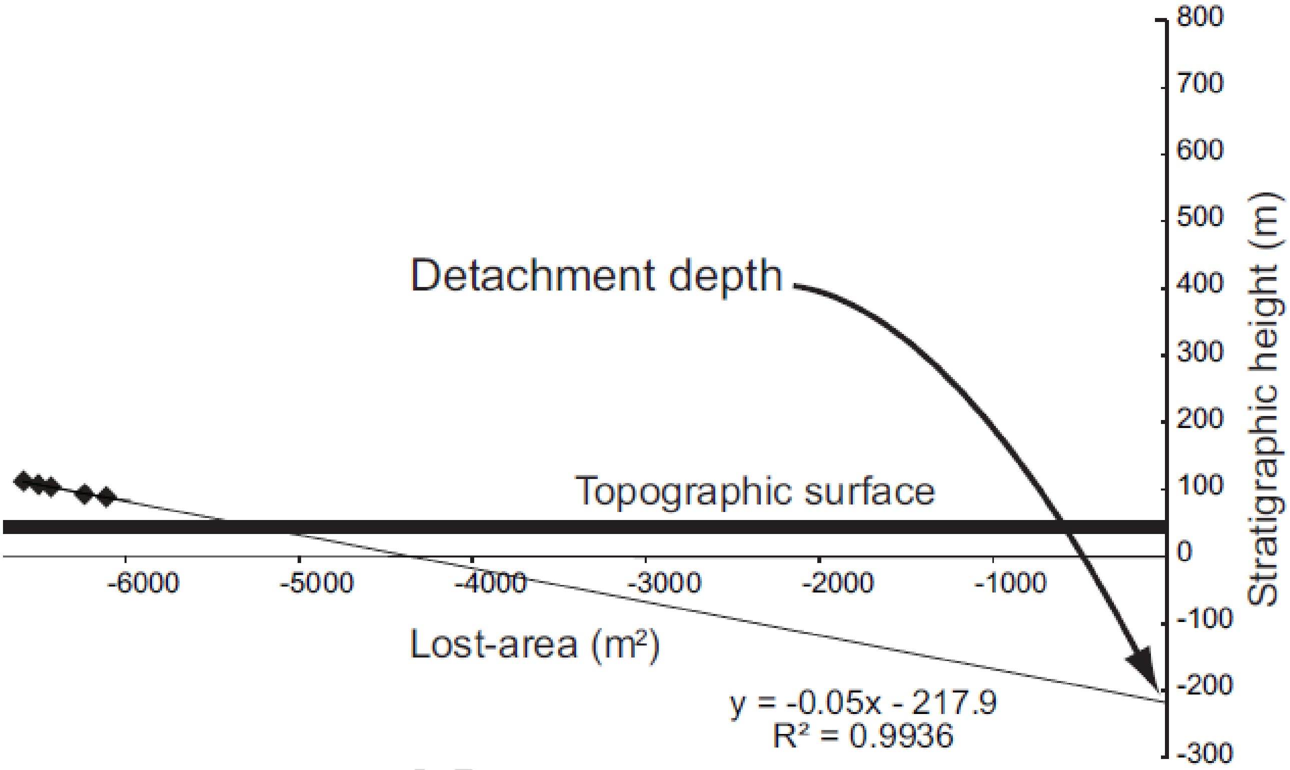
Detachment depth
Topographic surface
-6000
-5000
-4000
-3000
-2000
-1000
Lost-area (m²)
y = -0.05x - 217.9
R² = 0.9936
800
700
600
500
400
300
200
100
0
-100
-200
-300
Stratigraphic height (m)

Fig. 29

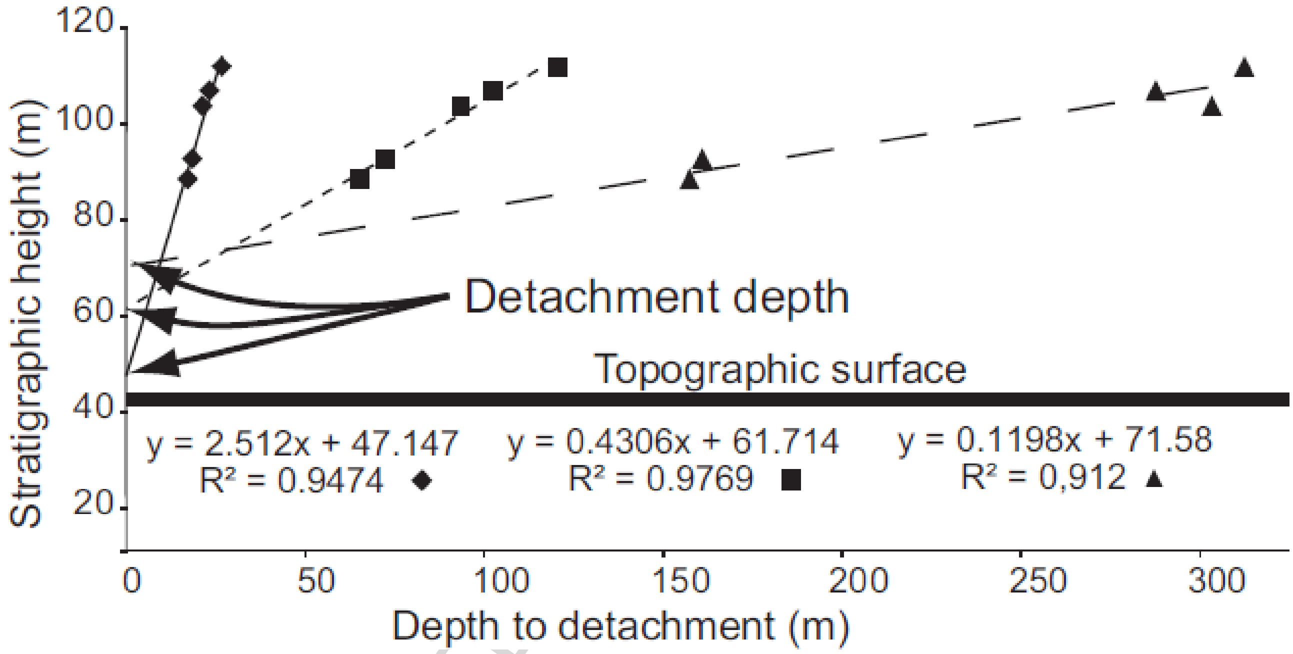
120
100
80
60
40
20
Stratigraphic height (m)
0
50
100
150
200
250
300
Depth to detachment (m)
Detachment depth
Topographic surface
y = 2.512x + 47.147
R² = 0.9474 ◆
y = 0.4306x + 61.714
R² = 0.9769 ■
y = 0.1198x + 71.58
R² = 0,912 ▲

Fig. 30

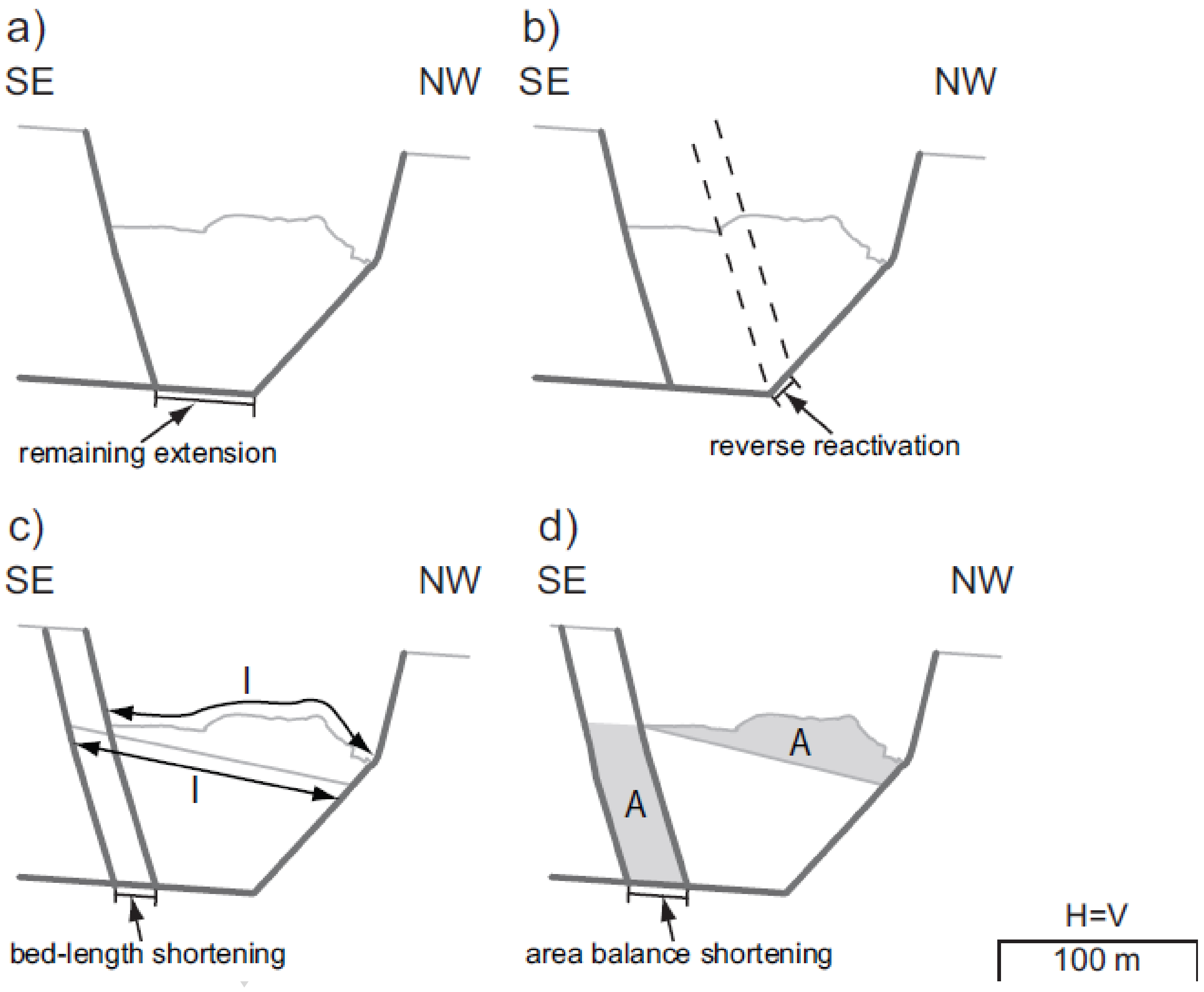
a)
SE
NW
remaining extension
b)
SE
NW
reverse reactivation
c)
SE
NW
l
l
bed-length shortening
d)
SE
NW
A
A
area balance shortening
H=V
100 m

Fig. 31

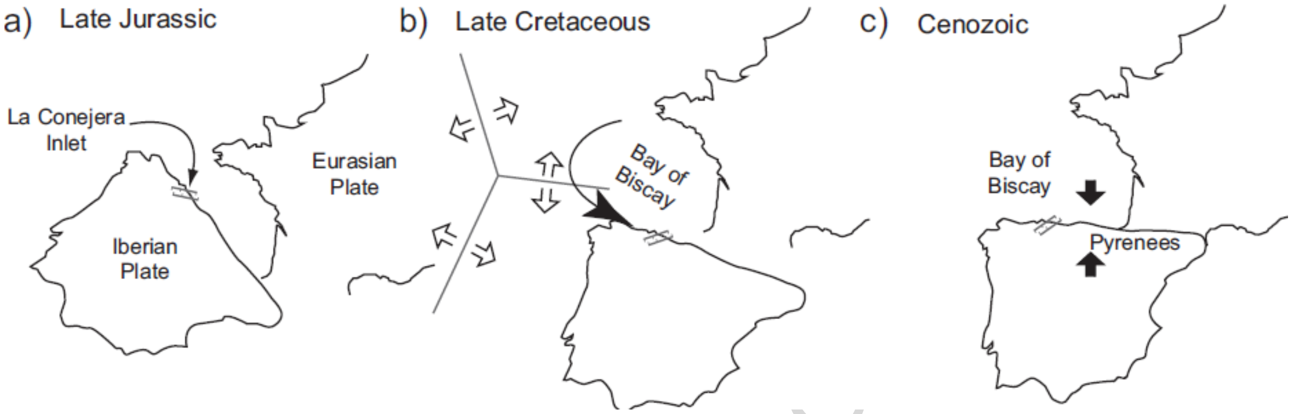
a) Late Jurassic
La Conejera Inlet
Iberian Plate
Eurasian Plate
b) Late Cretaceous
Bay of Biscay
c) Cenozoic
Bay of Biscay
Pyrenees

Fig. 32

Table 1

Fold	Type	Axis	Interlimb angle (º)	Amplitude* (m)	Half-wavelength (m)	Distance to fault** (m)	Axial trace dip (º)
I	Anticline	244/01	89	0.13	0.98	2.86	66[d]
II	Anticline	254/27	76	0.47	0.98	6.05	77[d]
III	Syncline	242/20[d]	95[d]	-	-	6.41	83[d]
IV	Anticline	-	68[d]	1.64	2.17	12.50	58[d]
V	Anticline	-	91[d]	0.35	0.72	5.76	77[d]
VI	Anticline	240/04	69	0.41	0.89	13.13	70[d]
VII	Syncline	245/02	73	0.46	0.77	13.95	81[d]
VIII	Anticline	-	88[d]	0.43	1.08	14.46	75[d]
IX	Anticline	230/02[d]	110[d]	0.38	1.11	34.77	74[d]
X	Anticline	068/10[d]	113[d]	-	-	34.32	84[d]
XI	Syncline	233/01	127	0.46	1.96	34.87	78[d]
XII	Anticline	246/05	105	0.87	2.80	49.47	82[d]
XIII	Anticline	-	110[d]	1.40	4.60	40.08	89[d]
XIV	Syncline	241/08	110	0.34	2.80	50.90	84[d]
XV	Anticline	247/09	117	0.57	5.58	58.78	83[d]
XVI	Syncline	255/05	108	0.75	4.57	62.01	86[d]
XVII	Anticline	254/04	107	3.04	16.22	87.73	88[d]
XVIII	Syncline	267/00	131	1.24	16.89	108.70	90[d]
XIX	Anticline	270/04	129	-	-	124.67	47[d]

Table 2

PRESENT-DAY		Current normal displacement along the main northern fault	58-66 m	
		Current normal displacement along the main southern fault	~45 m	
		Remaining extension	~50 m	
INVERSION	Ramp reactivation + Detachment reactivation + Buttressing	Total shortening (minimum estimation through area balance and bed-length)	20-28 m	
		Reverse reactivation of main northern fault (axial traces separation) [% of the total shortening]	12 m	43-60 %
		Detachment reactivation + buttressing (total minimum shortening – reverse reactivation) [% of the total shortening]	8-16 m	57-40 %
EXTENSION		Normal displacement along the main northern fault prior to compression (current displacement + fault-bend fold axial traces separation)	~70-78 m	
		Normal displacement along the main southern fault prior to compression (equal to the current one)	~45 m	
		Total extension prior to compression (minimum)	~70-78 m	

Highlights:

-Detailed structural analysis of a buttressing field example.

-Extension and compression values estimated through forward modelling.

-Detachment depth calculated for main fault.

-Extensional event related to the opening of the Bay of Biscay.

-Positive inversion tectonics event associated with the Pyrenees formation.